Molecular Biology of the Cell
Vol. 19, 2802–2817, July 2008

Dynamic Movement of the Calcium Sensor STIM1 and the Calcium Channel Orai1 in Activated T-Cells: Puncta and Distal Caps

Valarie A. Barr,* Kelsie M. Bernot,* Sonal Srikanth,†‡ Yousang Gwack,†‡ Lakshmi Balagopalan,* Carole K. Regan,* Daniel J. Helman,* Connie L. Sommers,* Masatsugu Oh-hora,† Anjana Rao,† and Lawrence E. Samelson*

*Laboratory of Cellular and Molecular Biology, National Cancer Institute, Bethesda, MD 20892-4256; and †Department of Pathology, Harvard Medical School and the Immune Disease Institute, Boston, MA 02115

Submitted February 13, 2008; Revised April 8, 2008; Accepted April 17, 2008
Monitoring Editor: Carl-Henrik Heldin

The proteins STIM1 and Orai1 are the long sought components of the store-operated channels required in T-cell activation. However, little is known about the interaction of these proteins in T-cells after engagement of the T-cell receptor. We found that T-cell receptor engagement caused STIM1 and Orai1 to colocalize in puncta near the site of stimulation and accumulate in a dense structure on the opposite side of the T-cell. FRET measurements showed a close interaction between STIM1 and Orai1 both in the puncta and in the dense cap-like structure. The formation of cap-like structures did not entail rearrangement of the entire endoplasmic reticulum. Cap formation depended on TCR engagement and tyrosine phosphorylation, but not on channel activity or Ca^{2+} influx. These caps were very dynamic in T-cells activated by contact with superantigen pulsed B-cells and could move from the distal pole to an existing or a newly forming immunological synapse. One function of this cap may be to provide preassembled Ca^{2+} channel components to existing and newly forming immunological synapses.

INTRODUCTION

T-cell activation in response to antigen induces and requires the elevation of intracellular Ca^{2+} (Hogan *et al.*, 2003; Quintana *et al.*, 2005; Feske, 2007). T-cell receptor (TCR) engagement leads to activation of well-documented signal transduction pathways that cause a rapid release of Ca^{2+} from the endoplasmic reticulum (ER; Samelson, 2002; Panyi *et al.*, 2004; Gwack *et al.*, 2007a). The depletion of Ca^{2+} from this internal store then leads to the opening of ion channels in the plasma membrane (PM) allowing an influx of Ca^{2+} from outside the cell. The store-operated channel responsible for Ca^{2+} influx in T-cells is known as the Ca^{2+} release–activated Ca^{2+} (CRAC) channel, which has been studied by electrophysiological techniques for many years (Lewis, 2001; Prakriya and Lewis, 2003; Cahalan *et al.*, 2007; Hewavitharana *et al.*, 2007; Hogan and Rao, 2007; Putney, 2007a).

This article was published online ahead of print in *MBC in Press* (http://www.molbiolcell.org/cgi/doi/10.1091/mbc.E08–02–0146) on April 30, 2008.

‡ Present Address: Department of Physiology, David Geffen School of Medicine at UCLA, Los Angeles, CA 90095-1751.

Address correspondence to: Lawrence E Samelson (samelson@helix.nih.gov).

Abbreviations used: APC, antigen-presenting cell; CRAC, Ca^{2+} release–activated Ca^{2+} channel; ER, endoplasmic reticulum; FRAP, fluorescence recovery after photobleaching; FRET, Förster resonance energy transfer; IS, immunological synapse; MEF, mouse embryonic fibroblast; PM, plasma membrane; TCR, T-cell receptor.

Sustained elevation of cytosolic Ca^{2+} is required for complete T-cell activation (Iezzi *et al.*, 1998; Lewis, 2001; Hogan *et al.*, 2003; Feske, 2007). High levels of intracellular Ca^{2+} are necessary to maintain the interaction between a T-cell and antigen-presenting cell (APC) that leads to formation of the specialized contact surface known as the immunological synapse (IS). Increased Ca^{2+} levels are also required for the activation of transcription factors. In particular, elevated Ca^{2+} maintains prolonged nuclear accumulation of nuclear factor of activated T-cells (NFAT) by activating the phosphatase calcineurin that dephosphorylates NFAT, allowing it to translocate to the nucleus and activate genes such as IL2 (Hogan *et al.*, 2003; Macian, 2005). Several hours of Ca^{2+} influx are required to complete the T-cell activation program, which involves expression of a large number of activation-associated genes (Lewis, 2001; Macian *et al.*, 2002; Hogan *et al.*, 2003).

Although sustained Ca^{2+} influx in T-cells has been studied for decades, the proteins involved have only been identified recently (Cahalan *et al.*, 2007; Feske, 2007; Gwack *et al.*, 2007a; Hewavitharana *et al.*, 2007; Hogan and Rao, 2007; Lewis, 2007; Putney, 2007b). Stromal-interacting molecule (STIM) was identified as an essential component for Ca^{2+} influx through CRAC channels by RNA interference (RNAi) screens in *Drosophila* and HeLa cells (Liou *et al.*, 2005; Roos *et al.*, 2005). Mammalian STIM1 is found predominantly in the ER and is a single-pass integral membrane protein with an N-terminal EF hand. STIM1 probably serves as the sensor that detects the depletion of Ca^{2+} stores. Further RNAi screens identified Orai1 or CRACM1 as a second essential component in

CRAC conductance (Feske *et al.*, 2006; Vig *et al.*, 2006b; Zhang *et al.*, 2006). Orai1 is a four-pass integral membrane protein found in the PM that forms the channel. Overexpression of STIM1 with Orai1 results in very large CRAC-like currents in *Drosophila* cell lines, Jurkat T-cells, RBL cells, and HEK293 cells (Mercer *et al.*, 2006; Peinelt *et al.*, 2006; Soboloff *et al.*, 2006; Zhang *et al.*, 2006). Recent studies have shown that Orai1 forms multimers and that targeted mutations in Orai1 alter the conductance properties of the CRAC channel (Prakriya *et al.*, 2006; Vig *et al.*, 2006a; Yeromin *et al.*, 2006; Gwack *et al.*, 2007b).

In order for ER-localized STIM1 to activate PM Orai1 channels, the two proteins must move to a common site and interact (Lewis, 2007; Putney, 2007b). Initial experiments showed that depletion of Ca^{2+} stores causes translocation of STIM1 into puncta near the PM with kinetics that precede channel opening (Liou *et al.*, 2005; Roos *et al.*, 2005; Mercer *et al.*, 2006; Wu *et al.*, 2006; Liou *et al.*, 2007), and that these puncta appear to correspond to sites of local Ca^{2+} entry (Luik *et al.*, 2006). STIM1 and Orai1 colocalize in these puncta (Luik *et al.*, 2006; Xu *et al.*, 2006; Li *et al.*, 2007), and aggregation of STIM1 can induce clustering of Orai1 (Xu *et al.*, 2006). Recent work has shown that STIM1 and Orai1 interact in cell-free pulldown assays and probably interact directly in live cells (Muik *et al.*, 2008). However, the complex formed at these sites is larger than just STIM1 and Orai1 combined (Varnai *et al.*, 2007). There has been some confusion over whether STIM1 actually inserts into the PM after store depletion. Some STIM1 resides in the PM in unstimulated cells (Manji *et al.*, 2000; Williams *et al.*, 2002), and externally applied anti-STIM1 antibodies have been reported to inhibit channel activation (Spassova *et al.*, 2006), but the relationship between PM STIM1 and the STIM1 that moves to puncta after store depletion is not clear. Many studies on STIM1 localization were performed with YFP-tagged fusion proteins that could not insert into the PM because of the YFP moiety (Hauser and Tsien, 2007) yet these fusion proteins were clearly capable of activating CRAC channels (Liou *et al.*, 2005; Baba *et al.*, 2006; Mercer *et al.*, 2006; Soboloff *et al.*, 2006; Wu *et al.*, 2006). Recent work has shown that STIM1 and Orai1 are in membrane contact points between the ER and PM and that movement of a complex containing the two proteins requires at least 10 nm between the two membranes (Varnai *et al.*, 2007). The current consensus is that STIM1 senses the depletion of Ca^{2+} from ER stores and then moves to sites of ER- PM apposition where interactions between STIM1 and Orai1 cause the opening of CRAC channels composed of Orai1 protein subunits (Luik *et al.*, 2006; Vig *et al.*, 2006a; Wu *et al.*, 2006; Feske, 2007; Hogan and Rao, 2007; Lewis, 2007; Putney, 2007a; Varnai *et al.*, 2007).

We used confocal imaging techniques to visualize the dynamic movement of STIM1 and Orai1 after T-cell activation. We were particularly interested in demonstrating close interactions between fluorescently tagged versions of STIM1 and Orai1 using the technique of Förster resonance energy transfer (FRET). Soon after TCR engagement, we observed puncta containing STIM1 and Orai1. At later times after stimulation, we also observed an unexpected rearrangement of STIM1 and Orai1 into dense structures located on the distal side of the T-cell. These cap-like structures suggest interesting possibilities about CRAC dynamics and regulation.

MATERIALS AND METHODS

Antibodies

The monoclonal antibodies used to coat the coverslips, anti-CD3 (HIT3a and UCHT1) and anti-CD45 were obtained from BD Biosciences Pharmingen (San Diego, CA). The following antibodies were used for immunofluorescence: rabbit anti-calnexin and goat anti-ezrin (1:100; Santa Cruz Biotechnology, Santa Cruz, CA), mouse anti-phosphotyrosine 4G10 (1:300, Upstate, Lake Placid, NY). Rabbit anti-Orai1 polyclonal antibody was custom made by Open Biosystems (Huntsville, AL) against the C- terminal peptide of Orai1: CDHRGDHPLTPGSHYA, where the cysteine at the N-terminus was introduced for the purpose of coupling the peptide with a carrier. The antibody was purified using a peptide-conjugated affinity column. Affinity-purified anti-Orai1 was used at a 1:300 dilution. Specificity of the antibody was confirmed by immunostaining (Supplemental Figure S1). Rabbit anti-STIM1 polyclonal antibodies were generated (Open Biosciences) against a C-terminal peptide of human STIM1 (CDNGSIGEETDSSPGRKKFPLKIFKKPLKK, where the cysteine at the N-terminus was introduced for the purpose of coupling the peptide with a carrier protein). The antibody was purified using peptide-conjugated affinity column. STIM1 anti-serum and affinity-purified anti-STIM1 were used at a 1:600 dilution. Secondary antibodies used for detection of immunofluorescence, and PP2 and BAPTA/AM were obtained from Molecular Probes/Invitrogen (Eugene, OR). 2-APB, CCCP, blebbistatin, and thapsigargin were from Calbiochem (La Jolla, CA). All remaining chemicals were obtained from Sigma-Aldrich (St. Louis, MO).

Cell Lines, Constructs, and Transfections

JCam1.6 Lck-deficient Jurkat cells and Lck-reconstituted JCaM1.6 cells were the kind gift of Dr. Arthur Weiss (University of California, San Francisco, CA). These cells, wild-type (E6.1) Jurkat T-cells, and Raji B-cells were maintained in RPMI 1640 supplemented with 10% fetal bovine serum and antibiotics. Tissue culture reagents were from BioFluids (Rockville, MD). The ER marker M1-YFP was the kind gift of Dr. Mark Philips (New York University, New York, NY). The Orai1-YFP and STIM1-CFP constructs were cloned into XhoI and EcoRI restriction sites in mYFP-N1 and mCFP-N1 vectors. The Orai1 cDNA was amplified using 5′ primer CGCCTCGAGATGCATCCGGAGCCCGCC containing the ATG start codon immediately after the XhoI restriction site and the 3′ primer CAGAATTCGGGCATAGTGGCTGCCGGG lacking the termination codon. The STIM1 cDNA was amplified using 5′ primer CGCCTCGAGATGGATGTATGCGTCCGTCTT containing the ATG start codon immediately after the XhoI restriction site and 3′ primer GCGCAGAATTCGCTTCTTAAGAGGCTTCTTAAA lacking the termination codon. Both the clones were sequence verified. Untagged Orai1 was obtained by modifying the Orai1-YFP construct. In addition, Orai1 was cloned into the mYFP-C1 vector (YFP-Orai1); however Jurkat T-cells transfected with this construct did not show normal spreading when plated onto stimulatory coverslips, in contrast to results with Orai1-YFP. Nonetheless, both Orai1-YFP– and YFP-Orai–complemented SCID fibroblasts and STIM1-CFP–complemented mouse knockout fibroblasts (Supplemental Figure S2). Complementation assays were performed as described previously (Feske *et al.*, 2006). Briefly, fibroblasts from SCID patients were immortalized and transduced with either vector alone or one of the Orai1 constructs. Mouse embryonic fibroblasts (MEFs) were obtained from STIM1 knockout mice and transduced with either vector alone or one of the STIM1 constructs. Fibroblasts were grown directly on UV-sterilized coverslips and loaded with 3 μM fura-2/AM for 45 min at 22–25°C. For $[Ca^{2+}]_i$ measurements, cells were mounted in a RC-20 closed-bath flow chamber (Warner Instrument, Hamden, CT) and analyzed on an Axiovert S200 epifluorescence microscope (Carl Zeiss, Thornwood, NY) with OpenLab imaging software (Improvision, Waltham, MA). Cells were perfused in Ca^{2+}-free Ringer solution, and Ca^{2+} stores were passively depleted with 1 μM thapsigargin. Fura-2 emission was detected at 510 nm, with excitation at 340 and 380 nm, and Fura-2 emission ratios (340/380) were calculated after background subtraction at 5-s intervals. For each experiment, 340/380 ratios were calculated for 25–30 fibroblasts using Igor Pro (Wavemetrics, Lake Oswego, OR) analysis software. $[Ca^{2+}]_i$ was then calculated using the equation $[Ca^{2+}]_i = K * (R - Rmin)/(Rmax - R)$. Ca^{2+} influx rates were inferred from the maximal rate of rise in Ca^{2+} concentrations ($[Ca^{2+}]_i/dt$) after readdition of 0.2–2 mM $[Ca^{2+}]_o$. Transient transfections were performed using the Amaxa electroporation system (Amaxa Biosystems, Gaithersburg, MD).

$CD4^+$ T-cells were purified from lymph node single-cell suspensions using a mouse $CD4^+$ T-cell isolation kit and LS MACS separation columns (Miltenyi Biotec, Auburn, CA) according to the manufacturer's specifications. Cell purity was monitored by flow cytometry using a FACSCalibur (BD Biosciences, San Jose, CA) and FlowJo analysis software (Tree Star, Ashland, OR). Cells expressing the transgenic AND TCR (T-cell receptor; Vα11, Vβ3) were >80% (Kaye *et al.*, 1989).

Human T lymphocytes were prepared from peripheral blood of healthy donors as described previously (Laurence *et al.*, 2004). Briefly, mononuclear cells were isolated by Ficoll density gradient centrifugation. After washing, cells (10^6/ml) were stimulated at 37°C with 5 μg/ml phytohemagglutinin for 24 h. After two washes, cells were maintained in exponential growth phase in

RPMI-10% FCS supplemented with 20 ng/ml recombinant IL-2 for 5–6 d followed by washing. Flow cytometric analysis of cell surface markers showed predominantly T-cells (>90%).

Spreading Assays

Spreading assays were performed as described earlier (Bunnell *et al.*, 2003). Briefly, polylysine-covered four-chambered glass coverslips (LabTek II, Nunc/Nalgene, Rochester, NY) were coated with 10 μg/ml antibody (anti-CD3 HIT3a, anti-CD3 UCHT1, anti-CD45, or anti-CD3 plus anti-CD28 for peripheral blood lymphocytes [PBLs]). For immunofluorescent staining, the chambers were loaded with 300 μl of imaging buffer (normal media without phenol red supplemented with 25 mM HEPES, pH 7.0) and warmed. Cells were resuspended in imaging buffer at 2×10^5 cells/100 μl, injected into the bottom of the chamber, and incubated at 37°C. At the indicated times, Jurkat cells were fixed in 2.5% paraformaldehyde for 30 min, whereas PBLs were fixed in 1.2% paraformaldehyde. The cells were incubated with blocking buffer containing 0.1% NP-40 for 30 min and then incubated with primary antibody for 60 min. Antibody staining was detected with Alexa-conjugated secondary antibodies. For live cell imaging, the chambers were loaded with 900 μl of imaging buffer, placed on the microscope stage, and maintained at 37°C with a hot air blower and objective heater (Bioptics, Butler PA). Approximately 5000 cells were injected into the bottom of the chamber.

To visualize activated $CD4^+$ mouse T-cells, CH12 B-cells were pulsed with 10 μM MCC peptide (AnaSpec, San Jose, CA) for 1.5 h in DMEM + 10% fetal calf serum. The B-cells were then pelleted and resuspended in DMEM+ peptide but without serum, and plated onto polylysine-coated coverslips. After allowing the B-cells to adhere to the chamber for 30 min, the medium was replaced with imaging buffer. $CD4^+$ AND TCR cells were dropped onto the B-cells and allowed to activate 30 min at 37°C, followed by fixation with 2.4% paraformaldehyde for 30 min.

To visualize Jurkat T-cells interacting with superantigen pulsed B-cells, Raji B-cells were pulsed with 1–2 μg/ml staphylococcal enterotoxin E (SEE) toxin (Toxin Technology, Sarasota, FL) for 15 min in complete medium. After rinsing, the Raji cells were plated on polylysine-coated coverslips at 6×10^5 cells/chamber in serum-free media for 2 h. The medium was replaced with imaging buffer, the chamber was placed on the warm microscope stage, and Jurkat T-cells were injected into the chamber. For some experiments, the Raji B-cells were incubated for 20 min with 2 μg/ml CellTracer FarRed (Molecular Probes, Eugene, OR), rinsed, and placed in complete medium overnight before being pulsed with SEE toxin.

Imaging

Images from fixed cells were collected with a Zeiss 510 LSCM, using a 63× objective (Carl Zeiss). The movements of fluorescent protein in live cells were observed with a Zeiss Axiovert 200 microscope equipped with a Perkin Elmer-Cetus ERS 6FO Ultraview spinning disk confocal system (PerkinElmer, Shelton, CT), using a 63× objective and the images were recorded with an Orca-ERII CCD camera (Hamamatsu, Bridgewater, NJ). Photobleaching studies were performed on a Zeiss 510 LSCM using the 515-, 488-, and 458-nm laser lines for bleaching yellow fluorescent protein (YFP) and the 458- and 405-nm laser lines for bleaching cyan fluorescent protein (CFP).

FRET was measured by the donor-sensitized acceptor fluorescence technique on a Zeiss 510 LSCM (Carl Zeiss). Three sets of images were collected: donor fluorescence (458-nm excitation, 475–505-nm BP emission filter), FRET (458-nm excitation, 530-nm LP emission filter), and acceptor fluorescence (515-nm excitation, 530-nm LP emission filter).

Image Processing

Imaris 4.2 (Bitplane, Zurich Switzerland) was used for most image processing and to produce 3D sectional views and 3D rendered images. Maximum intensity projections of each z-stack at each time point were prepared in Imaris and exported as avi movies. IP lab 3.6 (Scanalytics, Fairfax, VA) was used for image math functions including background subtraction and to prepare mosaic movies. Adobe PhotoShop and Illustrator (Adobe Systems, San Jose, CA) were used to prepare composite figures. In most cases, scale bars and other notations stamped on the images were removed and replaced with more legible versions using Adobe Photoshop and Illustrator.

To quantify the different staining patterns, Imaris was used to produce tilted views of 3D projections of confocal z series. Each field was examined from several angles to view each cell relative to the phosphotyrosine clusters on the bottom of the cell. Only activated cells with phosphotyrosine clusters were counted; at least 94% of the cells in a view were activated. Cells that could not be clearly identified as having caps, hemispheres, or rings of STIM1 staining were counted as round cells. To determine the distribution of puncta and caps similar projections were examined, but only cells with caps or puncta were analyzed. To quantify the effects of the various inhibitors and cells lines similar projections were made, but only cells with clearly defined caps were counted.

For calculating FRET efficiency, the FRET image was corrected for bleed-through of CFP emission into the YFP detection channel and cross-excitation of YFP by the 458-nm excitation laser using PFRET software (CircuSoft Instrumentation, Hockessin, DE). To perform the correction, we acquired reference images from Jurkat cells transfected with CFP or YFP alone. These images were used to generate calibration curves to calculate and remove the non-FRET components from the FRET image resulting in a corrected FRET image. The FRET efficiency was then calculated by the same software with the following equation: Efficiency = 1 − {Fluor. Intensity(CFP)/[Fluor. Intensity (CFP) + Fluor. Intensity(FRETcorrected)]}.

To reduce the possibility of obtaining false-positive FRET efficiencies, we calculated the FRET efficiency of negative control cells, that is, Jurkat cells coexpressing CFP and YFP, which should not interact. The average FRET efficiency from the negative control cells (~20%) was subtracted from the calculated FRET efficiency of samples imaged at the same time. Only the subtracted FRET efficiency levels are reported in the results. The average FRET efficiency of a positive FRET control consisting of CFP and YFP in a single construct was 19% after subtraction of the negative control.

Photobleaching calculations were performed with Excel (Microsoft, Redmond, WA). The prebleach fluorescence was normalized to 100%. Graphs were prepared with KaleidaGraph (Synergy Software, Reading, PA). The mobile fraction was calculated as follows (Ellenberg *et al.*, 1997; Brandizzi *et al.*, 2002): Mobile Fraction = [(Fluor Intensity(Bleach ROI) plateau after recovery − Fluor Intensity(Bleach ROI) post bleach)/(Fluor Intensity(Bleach ROI) prebleach − Fluor Intensity(Bleach ROI) post bleach)] ∗ (Fluor Intensity (Unbleached ROI) prebleach/Fluor Intensity(Unbleached ROI) end of experiment), where ROI is region of interest.

Flow Cytometry Analysis of Cytosolic Ca^{2+} Levels

Samples (1×10^6 cells/sample) were incubated with 5 M indo-1-acetoxymethylester (Indo-1-AM) and 0.5 mM probenecid at 37°C for 45 min in RPMI 1640 medium without supplements. The cells were then washed and resuspended in RPMI 1640 without phenol red containing 20 mM HEPES and 0.5 mM probenecid. The cells were incubated at 37°C before measurements and then stimulated with 500 ng/ml OKT3 antibody, 500 ng/mg anti-CD45 antibody, 1 μM thapsigargin, or 1 μM thapsigargin + 5 μg/ml Ionomycin. Indo-1 emission was detected simultaneously at 405 nm (405/20 bandpass filter) and 530 nm (530/30 bandpass filter with excitation at 355 nm by flow cytometry using an LSR II instrument (BD Biosciences). The data were processed and the Indo emission (405-nm/510-nm emission) was calculated using TreeStar FlowJo software.

RESULTS

After TCR Activation, Orai1-YFP and Stim1-CFP Are Seen in Puncta near the Stimulatory Surface

To examine the dynamics of STIM1 and Orai1 interactions after T-cell activation induced by TCR engagement, we observed Jurkat T-cells expressing either Orai1 conjugated to YFP (Orai1-YFP), STIM1 conjugated to CFP (STIM1-CFP), or both. To engage the TCR, cells were plated onto coverslips coated with stimulatory anti-CD3 antibodies, an experimental system that we have used extensively to study T-cell activation (Barr *et al.*, 2006; Bunnell *et al.*, 2001, 2002).

In unactivated Jurkat T-cells expressing Orai1-YFP, the protein was found at the PM (Prakriya *et al.*, 2006; Gwack *et al.*, 2007b; data not shown). This was also observed in cells activated by TCR engagement. Orai1-YFP was clearly visible in the PM of spreading lamellipodia, and was also seen in moving puncta near the stimulatory surface (Figure 1A, Movie 1). In Jurkat T-cells expressing STIM1-CFP plated onto coverslips coated with anti-CD45 antibodies that do not activate the TCR, STIM1-CFP was seen in an ER-like pattern that colocalized with ER markers such as calnexin (Rajagopalan *et al.*, 1994) as expected from previous studies (Figure 1B; Wu *et al.*, 2006; Liou *et al.*, 2007; Ross *et al.*, 2007). Activation of these cells resulted in formation of puncta containing STIM1-CFP (Supplemental Figure S3). In activated cells expressing both STIM1-CFP and Orai1-YFP, both proteins were present in puncta near the stimulatory surface (Figure 1C). The merge panel shows extensive colocalization of the two proteins in these clusters.

Although many studies have shown colocalization of STIM1 and Orai1 and the two proteins can be coimmunoprecipitated (Vig *et al.*, 2006a; Yeromin *et al.*, 2006; Gwack *et al.*, 2007b), a direct interaction after store depletion assessed by FRET has only been reported recently in HEK293 cells

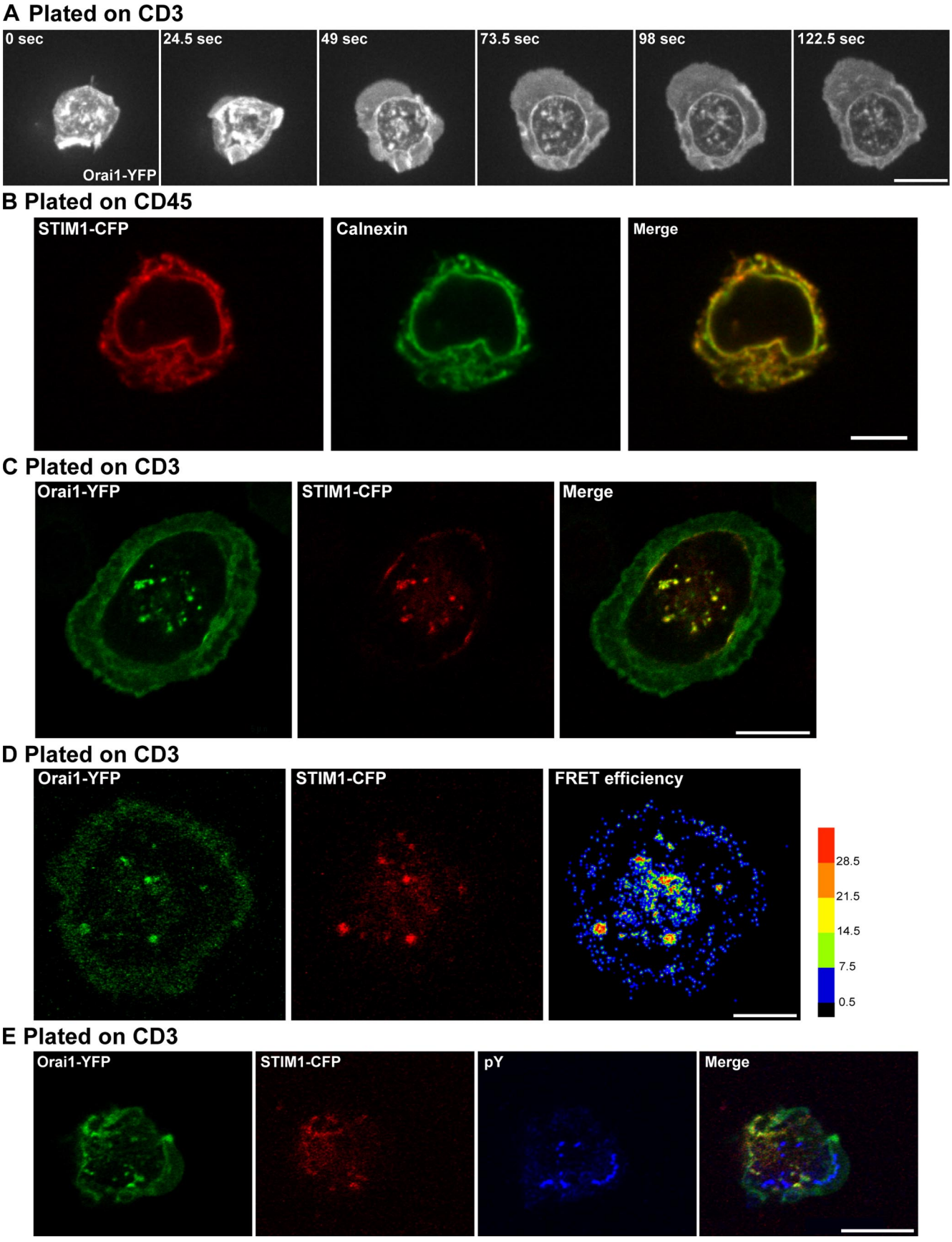

Figure 1. Orai1-YFP and STIM1-CFP puncta are induced by TCR activation in Jurkat T-cells. (A) A time series of E6.1 Jurkat T-cells expressing Orai1-YFP plated on anti-CD3–coated stimulatory coverslips and imaged with a spinning disk confocal system. A time series

(Muik *et al.*, 2008). We used FRET techniques to determine whether the two proteins interact in the puncta induced by TCR stimulation. The relative FRET efficiency between STIM1-CFP and Orai1-YFP was determined from sensitized emission images. The relative FRET efficiency shown in pseudocolor represents the calculated FRET efficiency of the sample minus the FRET efficiency of a negative FRET control consisting of nonconjugated CFP and YFP transfected together into Jurkat T-cells (Figure 1D). Subtracting the negative control FRET efficiency results in low calculated FRET efficiency values, but ensures that any positive FRET efficiency corresponds to real energy transfer. Accordingly, a positive FRET control consisting of CFP and YFP linked together gave a relative FRET efficiency of only 19%. Because the puncta containing STIM1-CFP and Orai1-YFP showed positive FRET indicating energy transfer, we conclude that the two proteins were within 10 nm of each other (Szollosi *et al.*, 1998).

The puncta containing interacting STIM1-CFP and Orai1-YFP did not colocalize with clusters containing phosphotyrosine that mark the sites of TCR clustering and activation (Figure 1E; Bunnell *et al.*, 2002). Thus, after TCR engagement, STIM1-CFP and Orai1-YFP closely interact in structures that are distinct from the signaling complexes that form at the activated TCR.

STIM1-CFP and Orai1-YFP Translocate into Cap-like Structures after TCR Activation

When Jurkat T-cells expressing STIM1-CFP were activated by contact with a stimulatory coverslip, there was another dramatic rearrangement of STIM1-CFP in addition to the interaction with Orai1-YFP in puncta. In cells transfected with STIM1-CFP alone, STIM1-CFP formed a dense, cap-like structure, usually at the pole of the cell farthest from the stimulatory surface, although sometimes STIM1-CFP collected along one side of the cell (Figure 2A, Movie 2). During this rearrangement, STIM1-CFP appeared to coalesce and rise along the side of the nucleus toward the top of the cell. In cells expressing both STIM1-CFP and Orai1-YFP, both proteins moved together into caps (Figure 2, B and C, Movie 3). A single cell often contained a dense cap on the top or side of the cell as well as puncta near the stimulatory surface. It was difficult to assess whether overexpressed Orai1-YFP could form caps in the absence of overexpressed STIM1-CFP because of the strong fluorescence of Orai1-YFP at the cell surface. STIM1-CFP and Orai1-YFP did not form caps in cells plated onto nonstimulatory coverslips coated with anti-CD45 antibodies. Under these conditions, Orai1-YFP was seen at the PM, while STIM1-CFP remained in the ER without forming puncta or translocating to a cap. (Figure 2D, Movie 4).

We used FRET imaging techniques to analyze the interaction of Orai1-YFP and STIM1-CFP in these unusual structures. We compared the relative FRET efficiency of cells fixed before caps had formed (2 min after activation) with that of cells with caps (15 min after activation; Figure 2E). There were similar values of positive FRET at both time points. There was little FRET between Orai1-YFP and STIM1-CFP in unactivated cells plated onto anti-CD45–coated coverslips (Figure 2E). In cells where both puncta and caps were visible, both structures showed positive FRET (Figure 2F, Movie 5), but the average FRET efficiency in caps was consistently higher than that in puncta (10.5% in caps vs. 5.9% in puncta).

The Mobility of STIM1-CFP and Orai1-YFP Decreases in the Caps

Because the development of the cap structures was impressive, yet unexpected, we focused our attention on them. We tested whether STIM1-CFP and Orai1-YFP were stably incorporated into caps using photobleaching techniques. First, we compared the fluorescence recovery after photobleaching (FRAP) of STIM1-CFP in unstimulated cells resting on a polylysine surface to that of STIM1-CFP in caps. We studied cells cotransfected with STIM1-CFP and untagged Orai1, because cotransfection of these two proteins is required for increased CRAC channel function (Mercer *et al.*, 2006; Peinelt *et al.*, 2006; Soboloff *et al.*, 2006; Zhang *et al.*, 2006). There was clear recovery of fluorescence from STIM1-CFP in the ER of unstimulated cells resting on polylysine, but little recovery of STIM1-CFP fluorescence when the bleached region was part of a cap structure in stimulated cells (Figure 3, A and C). The calculated mobile fraction of STIM1-CFP decreased from 52 ± 5% in the ER of unstimulated cells to 26 ± 4% in caps in stimulated cells.

We then used FRAP to determine the molecular mobility of Orai1-YFP. To be sure we could differentiate Orai-YFP in the PM from that in caps, we used cells cotransfected with STIM1-CFP to monitor cap location. In unactivated cells resting on polylysine, there was clear recovery of Orai1-YFP fluorescence, whereas Orai1-YFP in a cap with STIM1-CFP showed less recovery (Figure 3, B and D). The calculated mobile fraction of Orai1-YFP decreased from 61 ± 6% in unstimulated cells to 41 + 5% in cap structures (Figure 3D). These data show that once STIM1 and Orai1 accumulate in a cap, their mobility is significantly reduced, indicating that the caps are relatively stable structures.

Endogenous STIM1 and Orai1 Formed Caps after TCR Stimulation of Untransfected Jurkat T-cells

To determine whether redistribution of STIM1 and Orai1 and cap formation occurred in nontransfected cells, we examined the localization of both proteins by immunofluorescence in E6.1 Jurkat T-cells fixed after plating onto stimulatory coverslips. The cells were also stained with anti-phosphotyrosine antibodies to mark the sites in contact with the stimulatory surface. Figure 4A shows tilted side views of immunostained cells that show the location of STIM1 staining in relationship to the phosphotyrosine staining at the coverslip (Figure 4A). In cells fixed and stained 2 min after

Figure 1 (cont). consists of Z stacks from selected time points displayed as maximum intensity projections. The 0 time point corresponds to the first image in the series, which is not necessarily the first contact with the coverslip. Bar, 10 μm. (B) Cells expressing STIM1-CFP (red) were plated on anti-CD45–coated nonstimulatory coverslips, fixed after incubation at 37°C for 2 min, and immunostained with anti-calnexin antibodies (green). Bar, 10 μm, confocal section ~4 μm from bottom of cell. (C) Cells expressing Orai1-YFP (green) and STIM1-CFP (red) were plated on stimulatory coverslips and fixed after incubation at 37°C for 15 min. Bar, 10 μm, confocal section ~1 μm from coverslip. Colocalized proteins in puncta appear yellow in the merged image (D) FRET analysis of Orai1-YFP (green) and STIM1-CFP (red) fixed 15 min after plating on a stimulatory coverslip. The right panel shows relative FRET efficiency values presented as a pseudocolor scale. Relative FRET efficiency is defined as the calculated FRET efficiency minus the average FRET efficiency of free CFP and YFP in Jurkat cells fixed and imaged at the same time as the experimental samples. Bar, 5 μm confocal section ~1.5 μm from coverslip. (E) Cells expressing Orai1-YFP (green) and STIM1-CFP (red) were plated on a stimulatory coverslip, fixed after incubation at 37°C for 2 min, and immunostained with anti-phosphotyrosine antibodies (blue). Bar, 10 μm, confocal section ~1 μm from coverslip.

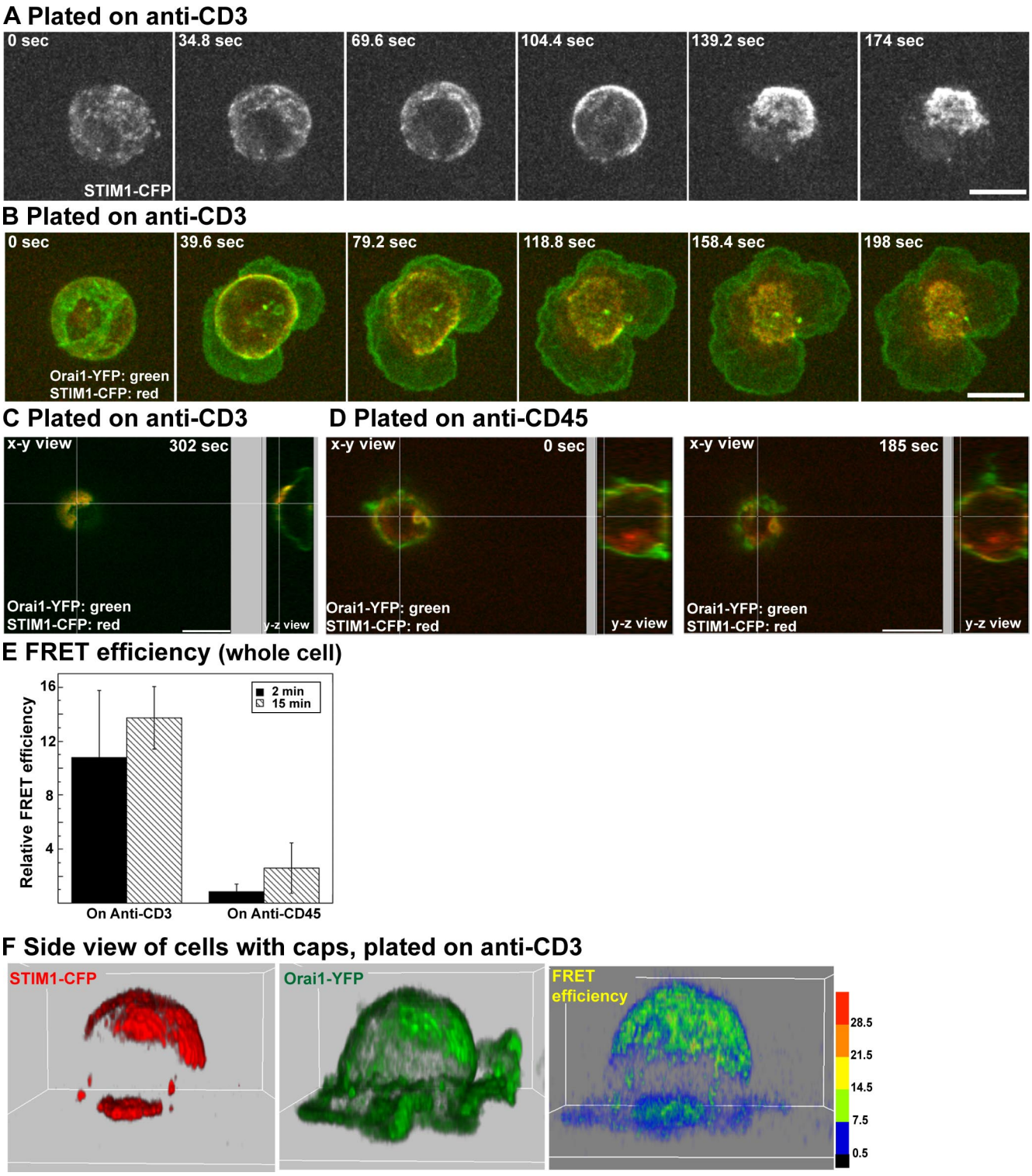

Figure 2. STIM1-CFP and Orai1-YFP form caps after TCR activation. (A) A time series of an E6.1 Jurkat T-cell expressing STIM1-CFP plated onto a stimulatory coverslip and imaged with a spinning disk confocal system. Bar, 7 μm. (B) A time series of a cell expressing STIM1-CFP (red) and Orai1-YFP (green) plated onto a stimulatory coverslip. Bar, 7 μm. (C) 3D section view of a cell expressing STIM1-CFP (red) and Orai1-YFP (green) plated onto a stimulatory coverslip. A single confocal x-y slice is shown in the main view, and the y-z projection is displayed on the right side. The last time point with a well-developed cap is shown. Bar, 10 μm (D) 3D section view of a cell expressing STIM1-CFP (red) and Orai1-YFP (green) plated onto a nonstimulatory coverslip coated with anti-CD45 antibodies. A single confocal x-y slice is shown in the main view, and the y-z projection is displayed on the right side. The first and last time points are shown. Bar, 10 μm. (E) FRET efficiency values in cells fixed at 2 min and cells fixed at 15 min plated on stimulatory (anti-CD3: 2 min, n = 22; 15 min, n = 26) and nonstimulatory (anti-CD45; 2 min, n = 17; 15 min, n = 11) coverslips. Relative FRET efficiency for the cell is defined as the calculated FRET efficiency from the z-section showing the most FRET in a given cell minus the average FRET efficiency of CFP and YFP in Jurkat cells fixed and imaged at the same time as the experimental samples. (F) 3D projection of cells expressing Orai1-YFP (green) and STIM1-CFP (red) fixed 15 min after plating on a stimulatory coverslip. The right panel shows relative FRET efficiency values on a pseudocolor scale.

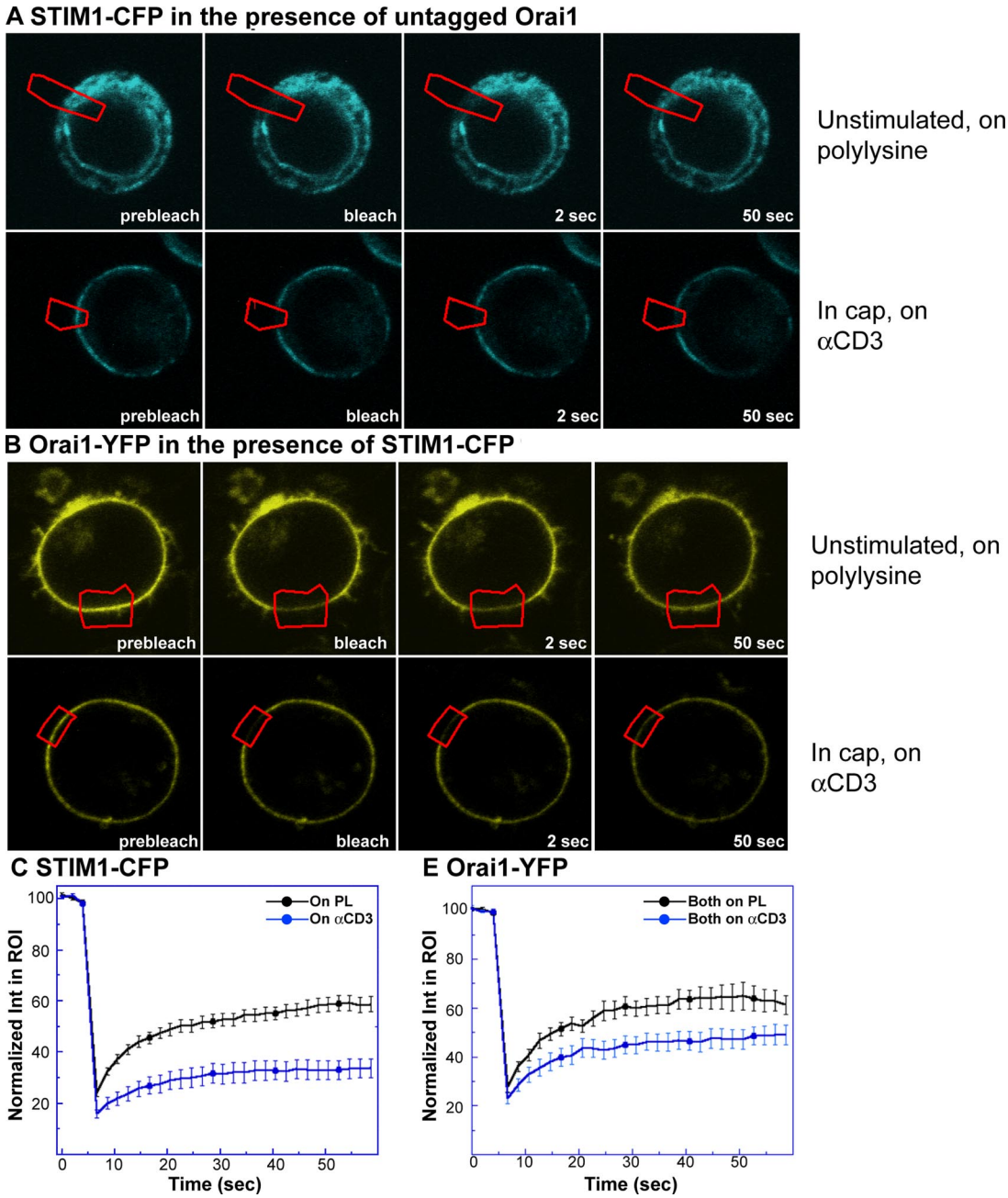

Figure 3. STIM1-CFP and Orai1-YFP show decreased mobility in caps. (A) FRAP of STIM1-CFP in unstimulated cells (top panels) or photobleaching of STIM1-CFP in a cap (bottom panels) in Jurkat T-cells expressing STIM1-CFP and untagged Orai1. Bleach region of interest (ROI) is shown in red. (B) FRAP of Orai1-YFP in unstimulated cells (top panels) or in a cap (bottom panels) in Jurkat T-cells expressing Orai1-YFP and STIM1-CFP. Bleach ROI is shown in red. (C) Average fluorescence recovery traces from photobleaching STIM1-CFP in cells expressing STIM1-CFP and untagged Orai1, on PL, n = 28, on anti-CD3, n = 21. Error bars, SEM. (D) Average fluorescence recovery traces from photobleaching Orai-YFP, on PL, n = 16, on anti-CD3, n = 18. Error bars, SEM.

plating, STIM1 was seen in a spherical, ER-like distribution around the nucleus with the flattened bottom of the sphere near the coverslip in all cells. In contrast, in cells fixed 7 min after plating, STIM1 was seen in a variety of structures that are consistent with a time-dependant translocation of STIM1 toward the top of the cell. In some cells, STIM1 was found in rings above the coverslip (yellow arrow), whereas in others STIM1 appeared as a hemisphere with the lower edge pulled away from the coverslip (white arrow). In a few cells, STIM1 was in a cap at the top or side of the cell. In cells fixed at 14 min after plating, we saw the same STIM1 staining patterns, with a greater abundance of STIM1 caps. This progression of STIM1 staining patterns recapitulates the movement of STIM1-CFP seen in live cells. A tilted view of a field of cells is shown in Figure 4B with a yellow arrow pointing to a cell with a ring of STIM1 staining and a white arrow pointing to a cell with a hemisphere. In the same image, white arrowheads mark three cells with caps. The increase in STIM1 cap formation with time is presented in a graph showing the percentage of cells that were scored with round, hemi-

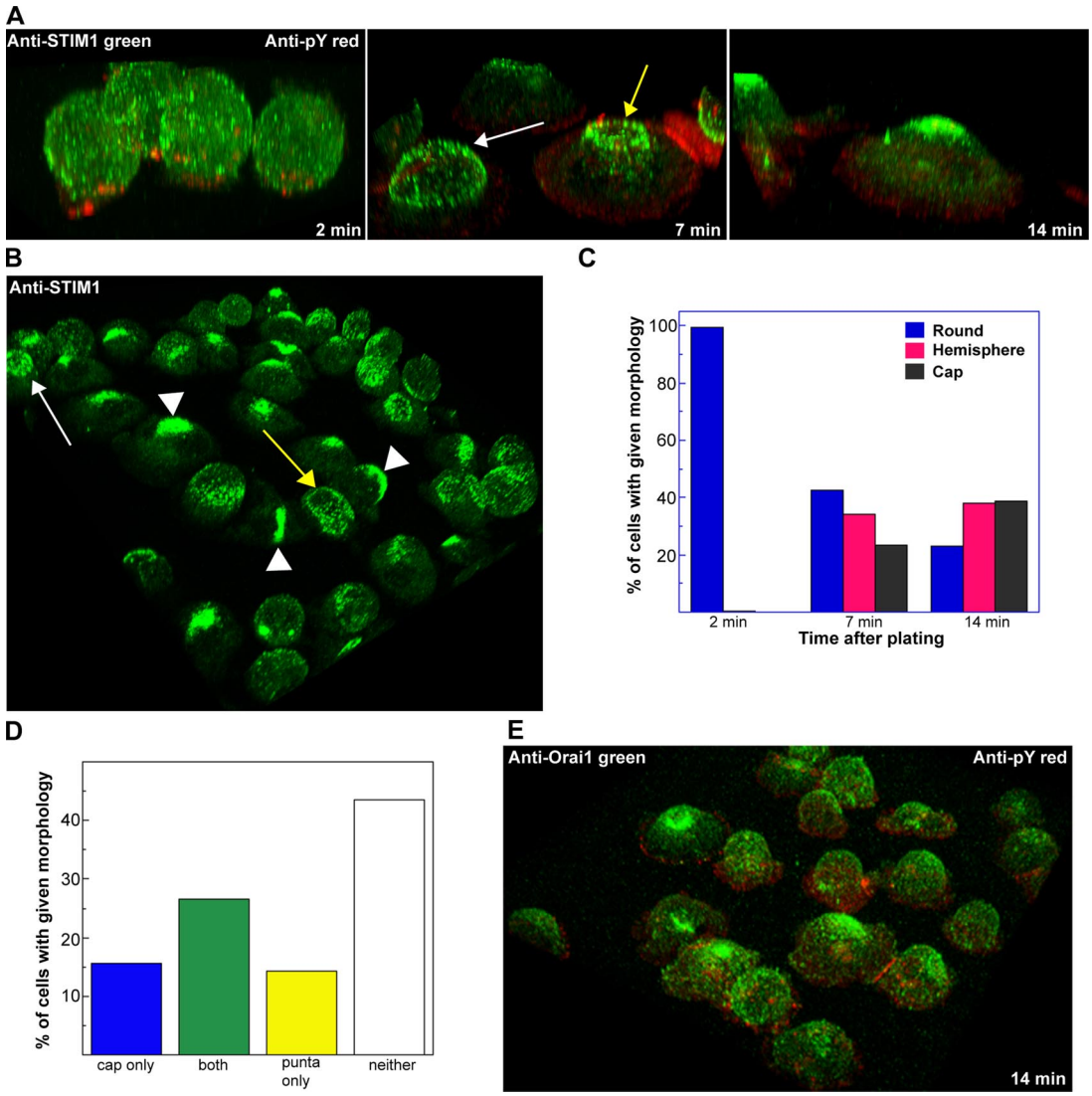

Figure 4. Endogenous STIM1 and Orai1 form caps after TCR activation of Jurkat T-cells. (A) E6.1 Jurkat T-cells were plated on a stimulatory coverslip, fixed after incubation at 37°C for 2, 7, or 14 min, and immunostained with anti-STIM1 (green) and anti-phosphotyrosine (red) antibodies. 3D projections are shown. In the 2-min panel, the STIM1 staining shows a round pattern and in the 7-min panel there is a cell with a hemisphere of STIM1 staining (white arrow) and another cell with a STIM1 ring (yellow arrow), whereas in the 14-min panel, the cells have STIM1 caps. (B) 3D projection of cells stained with anti-STIM1 (green) fixed 14 min after plating onto a stimulatory coverslip. The white arrow indicates a cell with a ring, and the yellow arrow marks a cell with a hemisphere of STIM1 staining. Arrowheads show three cells with STIM1 caps. (C) Graph of the percentage of cells showing each kind of STIM1 staining pattern at the three time points. Cells that could not be clearly identified as having caps, hemispheres, or rings of STIM1 staining were counted as round cells. Number of cells counted: 2 min, n = 187; 7 min, n = 192; and 14 min, n = 244. (D) Distribution of cells with caps and puncta fixed 15 min after plating onto a stimulatory coverslip. Cells that could not be clearly identified as having caps or puncta near the cell surface, including cells with rings or hemispheres, were labeled as neither. Number of cells examined: n = 699. (E) 3D projection of cells stained with anti-Orai1 (green) and anti-phosphotyrosine (red) antibodies fixed 14 min after plating onto a stimulatory coverslip. Caps are marked with arrowheads.

sphere/ring or cap-like STIM1 staining at different times after activation (Figure 4C). In this graph, any cell that did not show a clear ring, hemisphere or cap of STIM1 was counted as a round cell. Cap formation gradually increases over the course of activation. STIM1 puncta appeared before cap formation, with 12% of cells showing puncta at 2 min and 40% at 7 min and 14 min. Figure 4D shows the distribution of puncta and caps in cells fixed 15 min after activation. Cells with rings or hemispheres of STIM1 staining were not included in this analysis. Most cells with caps also had puncta, but there were a significant number of cells with only one type of STIM1 structure. Cap formation was also seen in immunofluorescent staining of Orai1 (Figure 4E). The specificity of the antisera was confirmed by comparison to staining in Jurkat cells with nonimmune serum and by comparing the staining in wild-type and knockout mouse cells (Supplemental Figure S1).

Cap Formation Is Not Driven by Reorganization of the ER

We then examined whether caps result from reorganization of the entire ER by observing the localization of the ER marker m1-YFP (Chiu *et al.*, 2002) in live Jurkat T-cells and calnexin in fixed Jurkat T-cells. The m1-YFP construct was

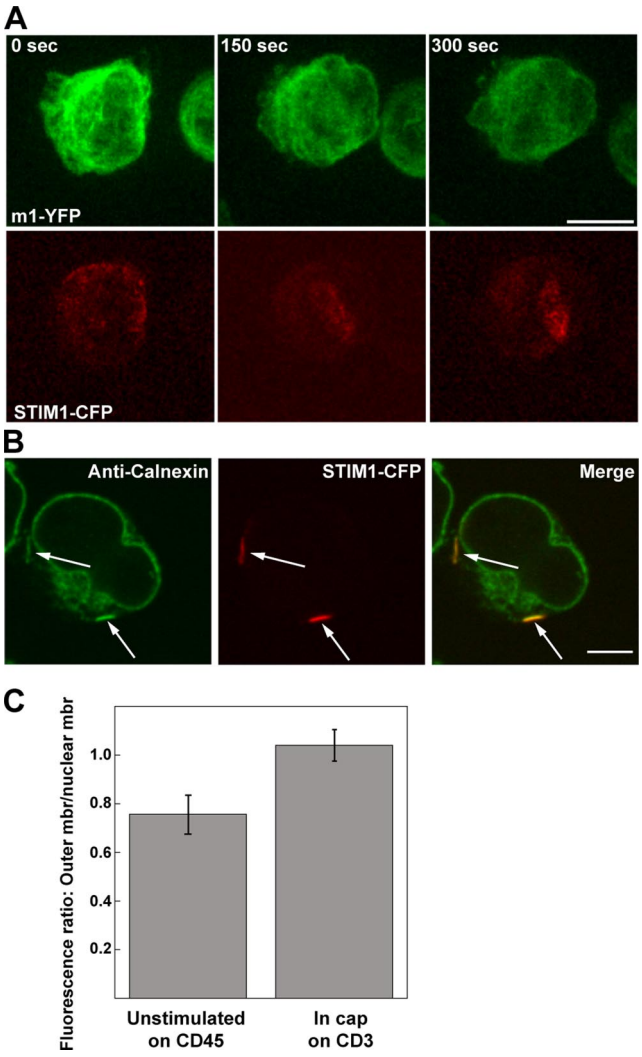

Figure 5. The ER remains relatively unperturbed during cap formation. (A) Jurkat T-cells cells expressing STIM1-CFP (red) and M1-YFP (green) were plated onto a stimulatory coverslip and imaged with a spinning disk confocal system. Three time points are shown. Bar, 10 μm. (B) Cells expressing STIM1-CFP (red) were plated on coverslips, fixed after incubation at 37°C for 15 min, and immunostained with anti-calnexin antibodies (green). A single confocal slice at the bottom of a cap is shown. Arrows mark increased calnexin staining in the two parts of the cap that are visible. Bar, 10 μm, confocal section ~4 μm from bottom of cell. (C) Quantification of calnexin redistribution. ROIs were drawn in the nuclear membrane and outer edge of the ER as marked by calnexin staining in unstimulated cells (n = 13) or in the nuclear membrane and cap in stimulated cells (n = 19). In unstimulated cells, the brightest calnexin staining is in the nuclear membrane, whereas in stimulated cells, the staining intensity in caps is as bright as the nuclear membrane.

expressed in the ER of transfected Jurkat cells, and most of the m1-YFP remained in unperturbed ER during T-cell activation (Figure 5A, Movie 6). However, some calnexin consistently accumulated at the site of the STIM1-CFP cap, albeit without major changes in ER structure. Figure 5B shows a confocal section near the bottom of a cap where the accumulation of calnexin in the cap is clear. We verified this redistribution by comparing the fluorescent intensity of calnexin immunostaining in an ROI at the outer edge of the cell to the intensity in an ROI at the nuclear membrane (Figure 5C). There was a statistically significant redistribution of calnexin ($p \leq 0.05$). In unstimulated cells, calnexin was more concentrated in the nuclear membrane than in the outer edge of the ER. In areas with caps, calnexin was evenly distributed. Nonetheless, it appears that cap formation is not driven by the general movement of the ER membranes.

An Intact Cytoskeleton Is Required For Normal Cap Formation

We then sought to determine the role of the cytoskeleton in STIM1 movement. STIM1 colocalizes with tubulin and plays a role in attaching ER membranes to the growing ends of microtubules (Baba *et al.*, 2006; Smyth *et al.*, 2007; Grigoriev *et al.*, 2008), so we reasoned that microtubules might play a role in cap formation. In cells treated with colchicine to disrupt microtubules, STIM1 localized to blebs that protruded from the top of the cell instead of forming a normal cap (Supplemental Figure S4, A and B). Evaluating the effects of disrupting the actin cytoskeleton was problematic because complete disassembly inhibits TCR activation, Ca^{2+} flux and blocks spreading of T-cells (Valitutti *et al.*, 1995; Bunnell *et al.*, 2001; Tskvitaria-Fuller *et al.*, 2003). We used a low dose of latrunculin to disrupt the actin network as visualized by actin-GFP (data not shown). Under these conditions, there was some TCR activation demonstrated by ZAP-70 clustering and modest Ca^{2+} flux (data not shown and Supplemental Figure S4H). In latrunculin-treated cells, STIM1-CFP and endogenous STIM1 formed patches on the plasma membrane that failed to coalesce or form a cap (Supplemental Figure 4, C and D). Many caps formed in cells treated with blebbistatin to inhibit myosin II (Straight *et al.*, 2003), although ring-like structures seemed more persistent in these cells (Supplemental Figure 4, E and F). Disruption of the cytoskeleton did not prevent STIM1 and Orai1 interaction and aggregation in response to TCR activation, but these molecules did not form normal cap structures. Myosin II inhibition slowed the progression from rings to caps but did not prevent cap formation.

Ca^{2+} Flux in the Absence of TCR Ligation Does Not Lead to Cap Formation

Next, we tested the effect of TCR engagement and other manipulations on cap formation. E6.1 Jurkat cells were activated on stimulatory or nonstimulatory coverslips, fixed, and immunostained for endogenous STIM1 (Figure 6, A–D). The percentage of cells with caps was then determined for all of the treatments (Figure 6L). Jurkat cells plated onto anti-CD45–coated coverslips did not form caps, as noted in our earlier experiments (Figure 6, B and L). The addition of thapsigargin to deplete ER stores led to the formation of puncta as previously reported (Supplemental Figure 5A; Liou *et al.*, 2005; Zhang *et al.*, 2005; Mercer *et al.*, 2006; Wu *et al.*, 2006; Xu *et al.*, 2006), but few caps formed (Figure 6, C and L). Increasing the Ca^{2+} flux by adding both thapsigargin and ionomycin did not increase cap formation (Figure 6, D and L). Thus, depletion of internal Ca^{2+} stores in the absence of TCR engagement did not lead to significant cap formation.

Influx of External Ca^{2+} Is Not Needed for Cap Formation

We performed similar experiments to analyze whether Ca^{2+} influx was required along with TCR activation (Figure 6, E–H). Cap formation was normal in cells treated with 2-APB to inhibit CRAC channel activity (Figure 6, E and L). Similarly, there was extensive cap formation in cells dropped into medium containing EGTA to chelate external Ca^{2+} (Figure 6, F and L). Even in cells pretreated with BAPTA to chelate internal Ca^{2+} and then plated into medium containing EGTA, cap formation was nearly normal (Figure 6, G

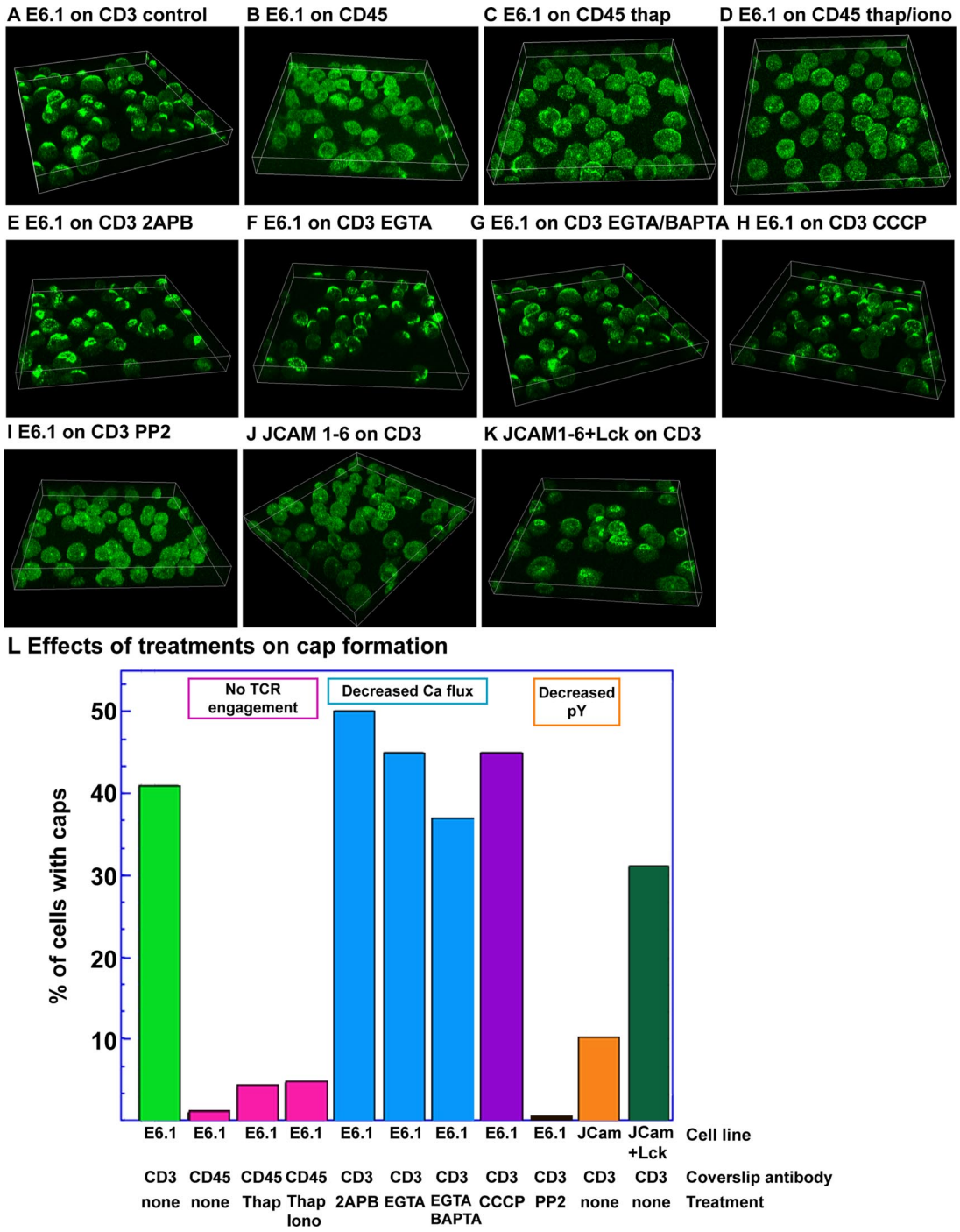

Figure 6. Cap formation requires TCR engagement and tyrosine phosphorylation but not channel activity or Ca^{2+} flux. Jurkat T-cells were plated onto coverslips, fixed after 15 min at 37°C, and immunostained with affinity-purified anti-STIM1 antibodies. A tilted view of a 3D projection of a field of cells is shown. (A) E6.1 cells on stimulatory anti-CD3 coverslips. (B) E6.1 cells on nonstimulatory anti-CD45 coverslips. (C) Two minutes after plating on nonstimulatory anti-CD45 coverslips, 1 μM thapsigargin was added to E6.1 cells. Cells were fixed 15 min later. (D) Two minutes after plating on anti-CD45 coverslips, 1 μM thapsigargin and 5 μg/ml ionomycin were added to E6.1 cells. Cells were fixed 15 min later. (E) E6.1 cells were pretreated with 50 μM 2-APB for 5 min and then plated onto anti-CD3 coverslips in the presence of 2-APB. (F) E6.1 cells were plated onto anti-CD3 coverslips in buffer containing 10 mM EGTA. (G) E6.1 cells were pretreated with 50 μM BAPTA-AM for 20 min and then plated onto anti-CD3 coverslips in buffer containing EGTA. (H) E6.1 cells were pretreated with 10 μM CCCP for 1 min and then plated onto anti-CD3 coverslips in the presence of 10 μM CCCP. (I) E6.1 cells were pretreated with 10 μM PP2 for 30 min and then plated onto anti-CD3 coverslips in the presence of PP2. (J) Lck-deficient JCaM1.6 Jurkat cells on anti-CD3 coverslips. (K) Lck-deficient JCaM1.6 Jurkat cells reconstituted with WT Lck on anti-CD3 coverslips. (J) Graph of the percentage of cells with caps after each treatment. Number of cells counted: control E6.1 cells on CD3, n = 699; E6.1 cells on CD45, n = 552; E6.1 cells on CD45 + thapsigargin, n = 487; E6.1 cells on CD45 + thapsigargin + ionomycin, n = 550; 2-APB–treated E6.1 cells on CD3, n = 489; EGTA-treated E6.1 cells on CD3, n = 362; EGTA+BAPTA–treated E6.1 cells on CD3, n = 327; CCCP-treated E6.1 cells on CD3, n = 445; PP2-treated E6.1 cells on CD3, n = 356; JCaM1.6 cells on CD3, n = 340; and Lck-reconstituted JCaM1.6 cells on CD3, n = 259.

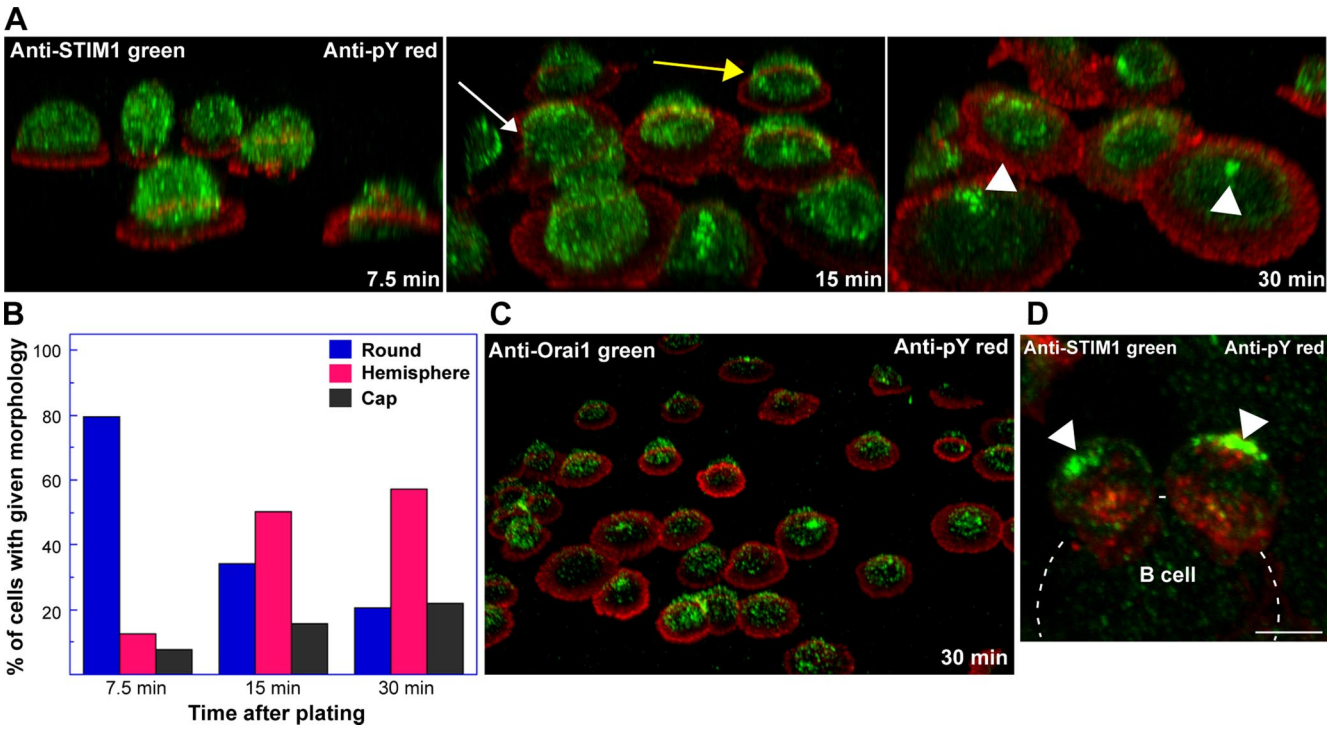

Figure 7. Caps of endogenous STIM1 and Orai1 form in human PLBs and mouse CD4 T-cells. (A) Human PBLs were plated on a stimulatory coverslip, fixed after incubation at 37°C for 7.5, 15, or 30 min, and immunostained with anti-STIM1 (green) and anti-phosphotyrosine (red) antibodies. 3D projections are shown. (B) Graph of the percentage of cells showing either round, ring/hemisphere or caps of STIM1 staining at the three time points. Number of cells counted: 7.5 min, n = 370; 15 min, n = 412, and 30 min, n = 451. (C) 3D projection of cells stained with anti-Orai1 (green) and anti-phosphotyrosine (red) antibodies fixed 30 min after plating onto a stimulatory coverslip. (D) Two mouse T-cells from AND TCR transgenic mice in contact with a peptide pulsed B-cell, fixed and immunostained with anti-STIM1 (green) and anti-phosphotyrosine (red) antibodies. Caps are indicated with arrowheads. Bar, 4 μm.

and L). Some studies have reported a connection between mitochondrial activity and maintenance of CRAC currents (Quintana *et al.*, 2006, 2007). We treated cells with CCCP to abolish mitochondrial potential, thus affecting both mitochondrial function and decreasing the magnitude of the CRAC current. Cap formation remained normal (Figure 6, H and L). In the presence of TCR ligation, Ca^{2+} flux is not needed.

Caps Do Not Form in the Absence of Tyrosine Phosphorylation

Because TCR ligation was required for cap formation, we then investigated whether downstream tyrosine phosphorylation was also required. Blocking tyrosine phosphorylation with the src family kinase inhibitor PP2 completely eliminated cap formation (Figure 6, I and L). Cap formation was also significantly reduced in JCaM1.6 cells that lack the tyrosine kinase, Lck (Figure 6, J and L). Without this proximal kinase, tyrosine phosphorylation and downstream signaling are greatly reduced (Straus and Weiss, 1992). Stable expression of wild-type Lck in JCaM1.6 cells restored cap formation (Figure 6, K and L). The effects of these perturbations on Ca^{2+} fluxes were confirmed by flow cytometry (Supplemental Figure 5B). Thus, treatments that reduced tyrosine phosphorylation inhibited cap formation.

Endogenous STIM1 and Orai1 Form Caps in Primary T-cells

To demonstrate that endogenous STIM1 and Orai1 formed caps in normal, nontransformed cells, we repeated our immunofluorescence studies with human PBLs fixed after plating onto coverslips coated with anti-CD3 and anti-CD28 antibodies. Again we saw changes in STIM1 localization consistent with cap formation, although smaller caps formed in PBLs (Figure 7A). Soon after plating, most cells showed a spherical distribution of STIM1. At later times, we observed a range of staining patterns, including rings (yellow arrow), hemispheres (white arrow), and caps (white arrowhead), and the number of cells with caps increased with increasing time after activation. Quantification of the change in STIM1 localization with time is shown in Figure 7B. Endogenous Orai1 also formed caps in PBLs (Figure 7C).

Numerous studies have shown that contact between a T-cell and an APC pulsed with a specific antigen leads to large-scale rearrangement of many proteins, resulting in the formation of an IS (Monks *et al.*, 1998; Delon *et al.*, 2002; Dustin, 2005). We were interested in how STIM1 and Orai1 might interact in the context of this intense membrane reorganization. Accordingly, we examined cap formation in $CD4^+$ T-cells from AND TCR transgenic mice, which possess only a single TCR that reacts with moth cytochrome c peptide (Kaye *et al.*, 1989). T-cells were activated by contact with MCC peptide–pulsed CH12 B-cells. In addition to staining of STIM1and Orai1 at the IS, caps were clearly visible in many of the T-cells (Figure 7D, white arrowheads). Caps did not form during interactions of T-cells with unpulsed B-cells (Supplemental Figure 6).

Localization of Distal Pole Markers and Polarity Markers in Cells Containing STIM1 Caps

Interactions with APCs also induce the formation of a protein complex distal to the contact site organized by ERM

(ezrin/radixin/moesin) proteins (Cullinan *et al.*, 2002). STIM1 contains an ERM domain so we examined the relationship between STIM1caps and the distal pole marker ezrin in PBLs. Although human PBLs do not form distal poles as readily as mouse T-cells, we were able to find some cells where ezrin accumulated on the distal side of the cell. Interestingly, ezrin did not overlap with STIM1; instead the two proteins formed side by side patches (Supplemental Figure 7A). PDZ-containing proteins are asymmetrically distributed in T-cells during migration and IS formation. The polarity markers scribble, numb, and PKCζ were associated with the distal pole in mouse T-cells (Ludford-Menting *et al.*, 2005; Chang *et al.*, 2007), so we looked for these proteins in STIM1 caps. In our human PBLs activated on coverslips, we did not see definitive segregation of any of these proteins in cells containing STIM1 caps (Supplemental Figure 7, B–D), indicating that caps can form in the absence of redistribution of these polarity markers.

Dynamic Caps Form after Interactions between Jurkat T-Cells and SEE Pulsed Raji B-Cells

We then sought to follow dynamics of cap formation during T-cell–B-cell interactions by observing live Jurkat T-cells transfected with STIM1-CFP and Orai1-YFP as they interacted with Raji B-cells that had been incubated with SEE toxin, a superantigen that stimulates T-cells by interacting with the Vβ region of the TCR (Herman *et al.*, 1991). SEE was used as an antigen substitute because the specific antigen for Jurkat T-cells is unknown. STIM1-CFP and Orai1-YFP translocated together after TCR engagement. Usually, they were seen near the contact surface between the two cells at the IS, often in clusters, and in a dense cap on the distal side of the T-cell away from the B-cell contact surface (Figure 8A, Movie 7). There were also cells that showed an accumulation of STIM1 and Orai1 at the IS without caps (Supplemental Figure 8A), as there were in T-cells activated by contact with dendritic cells (Lioudyno *et al.*, 2008). If no superantigen was present, there was no relocalization of Stim-CFP or Orai1-YFP (Supplemental Figure 8B).

The caps seemed more dynamic during T-cell–B-cell interactions than in the coverslip assays. Sometimes, the cap moved back to the IS after initially forming on the opposite side of the T-cell (Figure 8B, Movie 8). The caps were particularly mobile in cases where a T-cell interacted with multiple B-cells. STIM1 and Orai1 often moved together to several locations in the T-cell before finally forming a single cap distal to one B-cell (Figure 8C, Movie 9). However, we also observed T-cells with a central band of colocalized STIM1-CFP and Orai1-YFP, as if the T-cell was integrating signals from two B-cells so that the position of STIM1-CFP and Orai1-YFP reflected the locations of both B-cells (Figure 8D). Finally, there were cases when a T-cell that had formed a cap relative to one B-cell contacted a second B-cell, and the colocalized STIM1 and Orai1 in the cap moved to the contact site with the second B-cell, as if sending preassembled channel complexes to the newly forming IS (Figure 8E, Movie 10).

DISCUSSION

The fundamental elements needed for sustained Ca^{2+} influx through CRAC channels have recently been determined; the Ca^{2+} sensing protein STIM1 and the channel subunit protein Orai1 are both necessary and sufficient for CRAC channel activity. However little is known about the interaction of these two important proteins in lymphocytes after TCR stimulation. We used our assay for studying T-cell activation by confocal microscopy to follow the dynamics of both proteins in lymphocytes.

Soon after TCR activation of Jurkat T-cells, STIM1-CFP and Orai1-YFP colocalized in puncta near the stimulatory surface. These are superficially similar to STIM1 puncta containing Orai1 formed after thapsigargin-induced store depletion (Liou *et al.*, 2005; Zhang *et al.*, 2005; Mercer *et al.*, 2006; Wu *et al.*, 2006; Xu *et al.*, 2006). A recent study examined the localization of STIM1 and Orai1 T-cell activated by contact with dendritic cells pulsed with enterotoxin. The authors reported that STIM1, Orai1, and the TCR all colocalized at the IS (Lioudyno *et al.*, 2008). Our results in T-cells activated by super antigen–pulsed B-cells are consistent with their results in that we observed STIM1 and Orai1 accumulation at the contact surface that often overlapped with phosphotyrosine immunostaining marking the IS. However, in higher resolution images from cells activated on coverslips, it is clear that the clusters of STIM1 and Ora1 that appeared soon after TCR engagement are distinct from the signaling complexes that form at clustered TCRs. We also observed STIM1 and Orai1 clusters that were mobile and inside the cell. This indicates that STIM1 and Orai1 may interact at locations other than the PM contact sites.

Until recently it has not been clear whether the colocalization of STIM1 and Orai1 was a result of direct interaction between the two or indirect interaction in a complex. However, a new study has shown both by FRET and direct pulldown experiments that STIM1 and Orai1 do interact in thapsigargin treated HEK293 cells (Muik *et al.*, 2008). We have extended this result by using FRET techniques to demonstrate that STIM1 and Orai1 are in close contact in puncta formed in Jurkat T-cells in response to TCR stimulation. In agreement with their results, we also do not see significant FRET in unstimulated cells.

We also observed an unexpected additional translocation of STIM1 and Orai1. Both proteins colocalized in an unusual structure distal to the stimulatory surface that formed several minutes after TCR engagement. The timing of this translocation indicates that the cap-like structure forms after the initial signal transduction events leading to Ca^{2+} store depletion. Cap formation appears to be a normal consequence of TCR activation because it does not depend on overexpression of either STIM1 or Orai1 and occurs in nontransformed PBLs as well as $CD4^+$ mouse T-cells. A recent epifluorescence study described only an accumulation of STIM1 and Orai1 at the IS between T lymphocytes and dendritic cells (Lioudyno *et al.*, 2008). However, we were able to demonstrate caps in a variety of activated cells including mouse $CD4^+$ T-cells, human PBLs, and Jurkat cells. The colocalization and FRET data suggest that STIM1 and Orai1 come together before both migrate to the distal side of the T-cell. The relationship between caps and the puncta near the stimulatory surface is not clear, but we do not see evidence for exchange between the two pools. In particular, we do not see puncta coming together to form the cap or merging with the cap once it is formed. Also, many cells contain both puncta near the IS and a cap. Our FRET measurements showed that STIM1 and Orai1 remain in close contact throughout translocation as well as in the caps, indicating that channel activity could be possible throughout the process. Our FRAP experiments suggest that caps are relatively stable structures. Thus after TCR stimulation, STIM1 and Orai1 accumulate in a complex far-removed from the site of stimulation.

One possible mechanism for cap formation is large-scale rearrangement of the ER containing STIM1. We did not see a gross perturbation of the ER, which is consistent previous

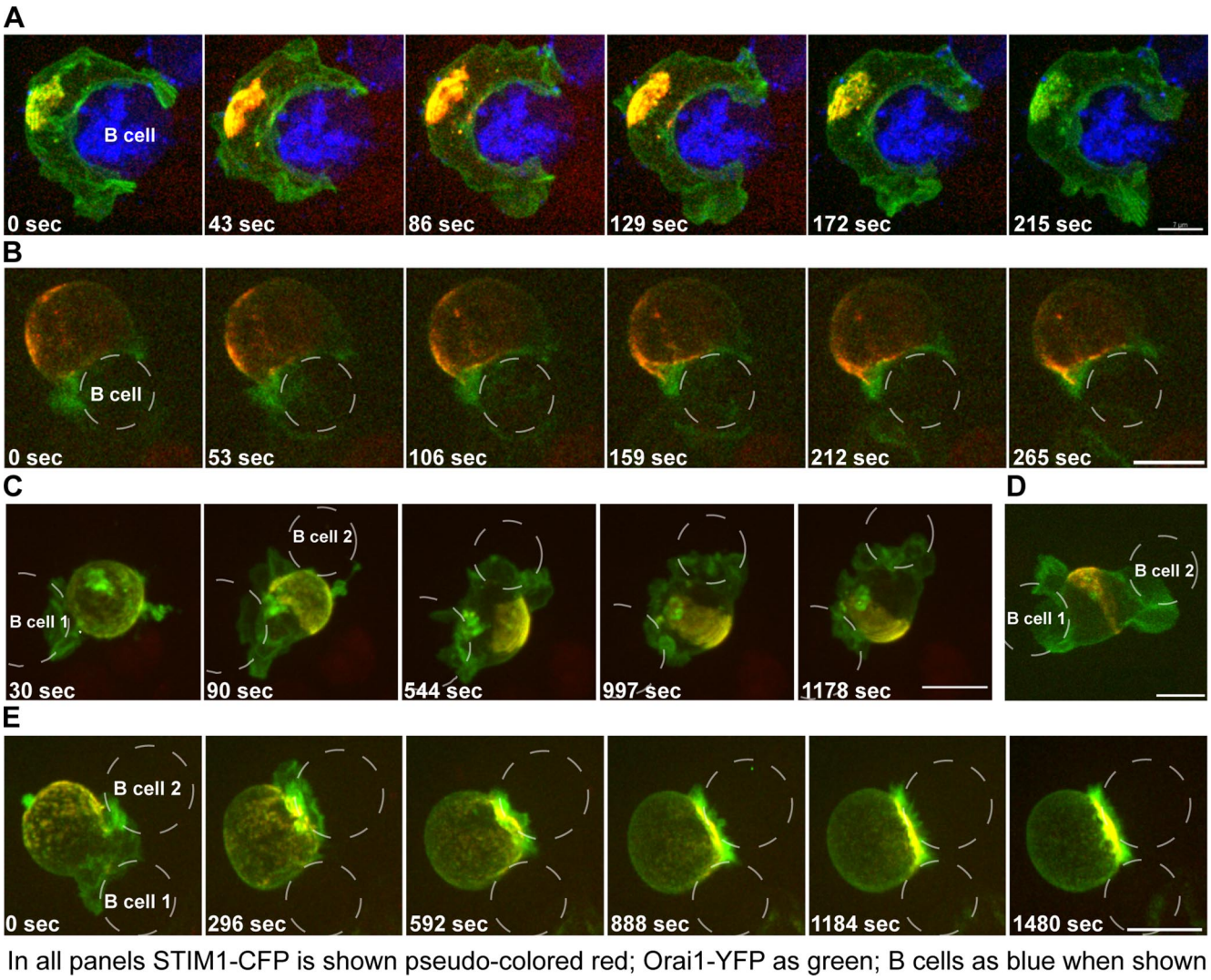

Figure 8. Dynamic caps in Jurkat T-cells activated by contact with superantigen-pulsed B-cells. Raji B-cells were pulsed with 1–2 μg/ml SEE toxin and were allowed to attach to polylysine-coated coverslips. E6.1 Jurkat T-cells expressing STIM1-CFP (red) and Orai-YFP (green) were added to the chamber and imaged with a spinning disk confocal system. The 0 time point corresponds to the first image in the series. Bar, 10 μm in all images. (A) Jurkat T-cell with prominent cap in contact with a B-cell. The B-cell (blue) has been visualized with CellTracker FarRed. (B) Jurkat T-cell in contact with a B-cell as the cap-like structure moves back to the contact site between the two cells. The B-cell was not stained. (C) Jurkat T-cell in contact with two B-cells as the cap forms oriented distal to the second B-cell. The B-cell channel is not shown. (D) Jurkat T-cell in contact with two B-cells with an accumulation of STIM1-CFP and Orai1-YFP between the two B-cells. The B-cells were not stained. (E) Jurkat T-cell in contact with two B-cells as the cap moves to the contact site with the second B-cell. The B-cell channel is not shown.

studies showing normal ER structure after Ca^{2+} store depletion (Ribeiro *et al.*, 2000; Baba *et al.*, 2006) and redistribution of STIM1 without bulk ER movement (Wu *et al.*, 2006). Cap formation did lead to a slightly altered distribution of calnexin that is consistent with the caps being formed of ER membrane closely apposed to the PM as is seen with STIM1 puncta induced by store depletion. We suggest that cap formation results from the movement of STIM1-containing membranes that remain part of the ER. However, STIM1-Orai1 complexes are larger than the two proteins combined (Varnai *et al.*, 2007), Orai1 itself is also part of a large macromolecular complex (Gwack *et al.*, 2007b), and TRPC1, TRPC4, and TRPC5 can all be coimmunoprecipitated with STIM1 (Lopez *et al.*, 2006; Ong *et al.*, 2007; Yuan *et al.*, 2007), so it seems likely that caps include other proteins in addition to STIM1 and Orai1. Although the localization of Stim1 is not exactly the same as that of ezrin at the distal pole, the organization of a network of ERM-containing proteins may be important for the sequestering of STIM1 and Orai1. Further experiments with mouse T-cells will be required to address the potential role of polarity-determining molecules.

STIM1 provides a direct link between ER membranes and the growing plus ends of microtubules. STIM1 comet-like structures are seen as ER tubules extend with the growing microtubules, but STIM1 comet movements cease after store depletion-induced clustering, indicating that the association with microtubules may be a distinct function from CRAC channel activation (Baba *et al.*, 2006; Grigoriev *et al.*, 2008). In HEK293 cells, microtubule depolymerizaton did decrease CRAC current, but it had little effect on store induced STIM1 clustering (Smyth *et al.*, 2007). In agreement with those re-

sults, we saw a modest inhibition of Ca^{2+} influx in Jurkat cells treated with colchicine, whereas STIM1 and Orai1 continued to aggregate at the distal side of the cell without forming normal caps. It is even more difficult to prove a direct role for the actin cytoskeleton in cap formation, because actin depolymerizaton has a direct effect on T-cell activation. No normal caps formed in cells treated with latrunculin, although we did see movement of STIM1 away from the ER and into PM patches containing Orai1. Investigations into the relationship of the cytoskeleton to STIM1 cap formation are continuing.

The formation of a cap at the distal pole of the cell has no counterpart in store depletion studies. Cap formation required signaling from the TCR, but did not require Ca^{2+} flux or channel activity, demonstrating that a unique rearrangement of STIM1 and Orai1 occurs during T-cell activation. One result of cap formation could be to affect the distribution of cytosolic Ca^{2+} in activated T-cells. Caps might provide a discrete Ca^{2+} source at the distal pole if the CRAC channels are active. Alternatively, the caps may be sequestering channels to reduce Ca^{2+} influx in areas outside of the IS. For example, if polarization of mitochondria, which import cytosolic Ca^{2+}, produces a Ca^{2+} gradient with low cytosolic Ca^{2+} near the IS (Quintana *et al.*, 2007), the CRAC channels in the cap would be in an area with the highest cytosolic Ca^{2+}. This would inactivate the CRAC channels in caps, whereas cap formation removes channels from the areas near the IS, enhancing the Ca^{2+} gradient.

Alternatively, the movement of the cap observed in some of the T-cell–B-cell interactions implies that it could provide a source of preassembled channels for subsequent IS formed by new T-cell–B-cell interactions or to resupply an existing IS. CRAC channels differ from similar channels in skeletal muscle where the dihydropyridine-sensitive PM channel is already in contact with the type 1 ryanodine receptor in the sarcoplasmic reticulum, allowing a fast Ca^{2+} response in muscle (Zalk *et al.*, 2007). Thus, the cap may serve as a repository of preformed channels that would allow more rapid T-cell responses when encountering additional antigen.

We saw varied cap behavior in our studies of T-cells interacting with B-cells. In this situation, cap formation may be involved in integrating the T-cell response to multiple APCs or targets. IS formation has also been examined in cases where a T-cell can interact with multiple APCs. Under these circumstances, the formation and stability of the IS depends on the relative strength of the TCR signal (Depoil *et al.*, 2005). Perhaps this phenomenon accounts for the variability of cap formation and stability in our assay.

T-cell activation leads to large changes in the structure of the cell, formation of macromolecular complexes and reorganization of the PM. One dramatic result, the formation of the IS at the contact site with APCs, has been studied intensively for many years without reaching a consensus on the function of this elaborate structure. We have now observed activation induced formation of a macromolecular structure containing the CRAC channel components, STIM1 and Orai1, on the distal side of the T-cell. Clustering of proteins at the PM is known to be involved in signal transduction in response to stimuli in many systems (Cho, 2006). Thus it seems likely that the clustering of STIM1 and Orai1 observed here is functionally relevant. This study is an important first step in the necessary molecular characterization of STIM1 and Orai1 complexes so that functional assays can be developed. Further investigation by those studying T-cell activation is needed to define the mechanism of formation and function of both the IS and the CRAC channel cap structure.

ACKNOWLEDGMENTS

We thank Dr. Alex Braiman for help with FRET calculations, Dr. Mark Philips for the tagged M1 constructs, Dr. Arthur Weiss for the JCam1.6 and Lck reconstituted JCam1.6 cell lines, and Barbara J. Taylor at the FACS CORE Facility. This research was supported by the Intramural Research Program of the National Institutes of Health (NIH), National Cancer Institute, Center for Cancer Research and by NIH Grants AI40127 and GM075256 to A.R..

REFERENCES

Baba, Y. *et al.* (2006). Coupling of STIM1 to store-operated Ca^{2+} entry through its constitutive and inducible movement in the endoplasmic reticulum. Proc. Natl. Acad. Sci. USA *103*, 16704–16709.

Barr, V. A. *et al.* (2006). T-cell antigen receptor-induced signaling complexes: internalization via a cholesterol-dependent endocytic pathway. Traffic *7*, 1143–1162.

Brandizzi, F., Snapp, E. L., Roberts, A. G., Lippincott-Schwartz, J., and Hawes, C. (2002). Membrane protein transport between the endoplasmic reticulum and the Golgi in tobacco leaves is energy dependent but cytoskeleton independent: evidence from selective photobleaching. Plant Cell *14*, 1293–1309.

Bunnell, S. C., Barr, V. A., Fuller, C. L., and Samelson, L. E. (2003). High-resolution multicolor imaging of dynamic signaling complexes in T cells stimulated by planar substrates. Sci STKE *2003*, PL8.

Bunnell, S. C., Hong, D. I., Kardon, J. R., Yamazaki, T., McGlade, C. J., Barr, V. A., and Samelson, L. E. (2002). T cell receptor ligation induces the formation of dynamically regulated signaling assemblies. J. Cell Biol. *158*, 1263–1275.

Bunnell, S. C., Kapoor, V., Trible, R. P., Zhang, W., and Samelson, L. E. (2001). Dynamic actin polymerization drives T cell receptor-induced spreading: a role for the signal transduction adaptor LAT. Immunity *14*, 315–329.

Cahalan, M. D., Zhang, S. L., Yeromin, A. V., Ohlsen, K., Roos, J., and Stauderman, K. A. (2007). Molecular basis of the CRAC channel. Cell Calcium *42*, 133–144.

Chang, J. T. *et al.* (2007). Asymmetric T lymphocyte division in the initiation of adaptive immune responses. Science *315*, 1687–1691.

Chiu, V. K., Bivona, T., Hach, A., Sajous, J. B., Silletti, J., Wiener, H., Johnson, R. L., 2nd, Cox, A. D., and Philips, M. R. (2002). Ras signalling on the endoplasmic reticulum and the Golgi. Nat. Cell Biol *4*, 343–350.

Cho, W. (2006). Building signaling complexes at the membrane. Science's Stke [Electronic Resource]: Signal Transduction Knowledge Environment *2006*, pe7.

Cullinan, P., Sperling, A. I., and Burkhardt, J. K. (2002). The distal pole complex: a novel membrane domain distal to the immunological synapse. Immunol. Rev. *189*, 111–122.

Delon, J., Stoll, S., and Germain, R. N. (2002). Imaging of T-cell interactions with antigen presenting cells in culture and in intact lymphoid tissue. Immunol. Rev. *189*, 51–63.

Depoil, D., Zaru, R., Guiraud, M., Chauveau, A., Harriague, J., Bismuth, G., Utzny, C., Muller, S., and Valitutti, S. (2005). Immunological synapses are versatile structures enabling selective T cell polarization. Immunity *22*, 185–194.

Dustin, M. L. (2005). A dynamic view of the immunological synapse. Semin. Immunol. *17*, 400–410.

Ellenberg, J., Siggia, E. D., Moreira, J. E., Smith, C. L., Presley, J. F., Worman, H. J., and Lippincott-Schwartz, J. (1997). Nuclear membrane dynamics and reassembly in living cells: targeting of an inner nuclear membrane protein in interphase and mitosis. J. Cell Biol. *138*, 1193–1206.

Feske, S. (2007). Calcium signalling in lymphocyte activation and disease. Nat. Rev. Immunol. *7*, 690–702.

Feske, S., Gwack, Y., Prakriya, M., Srikanth, S., Puppel, S. H., Tanasa, B., Hogan, P. G., Lewis, R. S., Daly, M., and Rao, A. (2006). A mutation in Orai1 causes immune deficiency by abrogating CRAC channel function. Nature *441*, 179–185.

Grigoriev, I. *et al.* (2008). STIM1 is a MT-plus-end-tracking protein involved in remodeling of the ER. Curr. Biol. *18*, 177–182.

Gwack, Y., Feske, S., Srikanth, S., Hogan, P. G., and Rao, A. (2007a). Signalling to transcription: store-operated Ca^{2+} entry and NFAT activation in lymphocytes. Cell Calcium *42*, 145–156.

Gwack, Y., Srikanth, S., Feske, S., Cruz-Guilloty, F., Oh-hora, M., Neems, D. S., Hogan, P. G., and Rao, A. (2007b). Biochemical and functional characterization of Orai proteins. J. Biol. Chem. *282*, 16232–16243.

Hauser, C. T., and Tsien, R. Y. (2007). A hexahistidine-Zn^{2+}-dye label reveals STIM1 surface exposure. Proc. Natl. Acad. Sci. USA *104*, 3693–3697.

Herman, A., Kappler, J. W., Marrack, P., and Pullen, A. M. (1991). Superantigens: mechanism of T-cell stimulation and role in immune responses. Annu. Rev. Immunol. *9*, 745–772.

Hewavitharana, T., Deng, X., Soboloff, J., and Gill, D. L. (2007). Role of STIM and Orai proteins in the store-operated calcium signaling pathway. Cell Calcium *42*, 173–182.

Hogan, P. G., Chen, L., Nardone, J., and Rao, A. (2003). Transcriptional regulation by calcium, calcineurin, and NFAT. Genes Dev. *17*, 2205–2232.

Hogan, P. G., and Rao, A. (2007). Dissecting ICRAC, a store-operated calcium current. Trends Biochem. Sci. *32*, 235–245.

Iezzi, G., Karjalainen, K., and Lanzavecchia, A. (1998). The duration of antigenic stimulation determines the fate of naive and effector T cells. Immunity *8*, 89–95.

Kaye, J., Hsu, M. L., Sauron, M. E., Jameson, S. C., Gascoigne, N. R., and Hedrick, S. M. (1989). Selective development of CD4+ T cells in transgenic mice expressing a class II MHC-restricted antigen receptor. Nature *341*, 746–749.

Laurence, A., Astoul, E., Hanrahan, S., Totty, N., and Cantrell, D. (2004). Identification of pro-interleukin 16 as a novel target of MAP kinases in activated T lymphocytes. Eur. J. Immunol. *34*, 587–597.

Lewis, R. S. (2001). Calcium signaling mechanisms in T lymphocytes. Annu. Rev. Immunol. *19*, 497–521.

Lewis, R. S. (2007). The molecular choreography of a store-operated calcium channel. Nature *446*, 284–287.

Li, Z., Lu, J., Xu, P., Xie, X., Chen, L., and Xu, T. (2007). Mapping the interacting domains of STIM1 and Orai1 in Ca^{2+} release-activated Ca^{2+} channel activation. J. Biol. Chem. *282*, 29448–29456.

Liou, J., Fivaz, M., Inoue, T., and Meyer, T. (2007). Live-cell imaging reveals sequential oligomerization and local plasma membrane targeting of stromal interaction molecule 1 after Ca^{2+} store depletion. Proc. Natl. Acad. Sci. USA *104*, 9301–9306.

Liou, J., Kim, M. L., Heo, W. D., Jones, J. T., Myers, J. W., Ferrell, J. E., Jr., and Meyer, T. (2005). STIM is a Ca^{2+} sensor essential for Ca^{2+}-store-depletion-triggered Ca^{2+} influx. Curr. Biol. *15*, 1235–1241.

Lioudyno, M. I., Kozak, J. A., Penna, A., Safrina, O., Zhang, S. L., Sen, D., Roos, J., Stauderman, K. A., and Cahalan, M. D. (2008). Orai1 and STIM1 move to the immunological synapse and are up-regulated during T cell activation. Proc. Natl. Acad. Sci. USA *105*, 2011–2016.

Lopez, J. J., Salido, G. M., Pariente, J. A., and Rosado, J. A. (2006). Interaction of STIM1 with endogenously expressed human canonical TRP1 upon depletion of intracellular Ca^{2+} stores. J. Biol. Chem. *281*, 28254–28264.

Ludford-Menting, M. J. *et al.* (2005). A network of PDZ-containing proteins regulates T cell polarity and morphology during migration and immunological synapse formation. Immunity *22*, 737–748.

Luik, R. M., Wu, M. M., Buchanan, J., and Lewis, R. S. (2006). The elementary unit of store-operated Ca^{2+} entry: local activation of CRAC channels by STIM1 at ER-plasma membrane junctions. J. Cell Biol. *174*, 815–825.

Macian, F. (2005). NFAT proteins: key regulators of T-cell development and function. Nat. Rev. Immunol. *5*, 472–484.

Macian, F., Garcia-Cozar, F., Im, S. H., Horton, H. F., Byrne, M. C., and Rao, A. (2002). Transcriptional mechanisms underlying lymphocyte tolerance. Cell *109*, 719–731.

Manji, S. S., Parker, N. J., Williams, R. T., van Stekelenburg, L., Pearson, R. B., Dziadek, M., and Smith, P. J. (2000). STIM1, a novel phosphoprotein located at the cell surface. Biochim. Biophys. Acta *1481*, 147–155.

Mercer, J. C., Dehaven, W. I., Smyth, J. T., Wedel, B., Boyles, R. R., Bird, G. S., and Putney, J. W., Jr. (2006). Large store-operated calcium selective currents due to co-expression of Orai1 or Orai2 with the intracellular calcium sensor, Stim1. J. Biol. Chem. *281*, 24979–24990.

Monks, C. R., Freiberg, B. A., Kupfer, H., Sciaky, N., and Kupfer, A. (1998). Three-dimensional segregation of supramolecular activation clusters in T cells. Nature *395*, 82–86.

Muik, M. *et al.* (2008). Dynamic coupling of the putative coiled-coil domain of ORAI1 with STIM1 mediates ORAI1 channel activation. J. Biol. Chem. *283*, 8014–8022.

Ong, H. L. *et al.* (2007). Dynamic assembly of TRPC1-STIM1-Orai1 ternary complex is involved in store-operated calcium influx. Evidence for similarities in store-operated and calcium release-activated calcium channel components. J. Biol. Chem. *282*, 9105–9116.

Panyi, G., Varga, Z., and Gaspar, R. (2004). Ion channels and lymphocyte activation. Immunol. Lett. *92*, 55–66.

Peinelt, C., Vig, M., Koomoa, D. L., Beck, A., Nadler, M. J., Koblan-Huberson, M., Lis, A., Fleig, A., Penner, R., and Kinet, J. P. (2006). Amplification of CRAC current by STIM1 and CRACM1 (Orai1). Nat. Cell Biol. *8*, 771–773.

Prakriya, M., Feske, S., Gwack, Y., Srikanth, S., Rao, A., and Hogan, P. G. (2006). Orai1 is an essential pore subunit of the CRAC channel. Nature *443*, 230–233.

Prakriya, M., and Lewis, R. S. (2003). CRAC channels: activation, permeation, and the search for a molecular identity. Cell Calcium *33*, 311–321.

Putney, J. W., Jr. (2007a). New molecular players in capacitative Ca^{2+} entry. J. Cell Sci. *120*, 1959–1965.

Putney, J. W., Jr. (2007b). Recent breakthroughs in the molecular mechanism of capacitative calcium entry (with thoughts on how we got here). Cell Calcium *42*, 103–110.

Quintana, A., Griesemer, D., Schwarz, E. C., and Hoth, M. (2005). Calcium-dependent activation of T-lymphocytes. Pfluegers Arch. *450*, 1–12.

Quintana, A., Schwarz, E. C., Schwindling, C., Lipp, P., Kaestner, L., and Hoth, M. (2006). Sustained activity of calcium release-activated calcium channels requires translocation of mitochondria to the plasma membrane. J. Biol. Chem. *281*, 40302–40309.

Quintana, A., Schwindling, C., Wenning, A. S., Becherer, U., Rettig, J., Schwarz, E. C., and Hoth, M. (2007). T cell activation requires mitochondrial translocation to the immunological synapse. Proc. Natl. Acad. Sci. USA *104*, 14418–14423.

Rajagopalan, S., Xu, Y., and Brenner, M. B. (1994). Retention of unassembled components of integral membrane proteins by calnexin. Science *263*, 387–390.

Ribeiro, C. M., McKay, R. R., Hosoki, E., Bird, G. S., and Putney, J. W., Jr. (2000). Effects of elevated cytoplasmic calcium and protein kinase C on endoplasmic reticulum structure and function in HEK293 cells. Cell Calcium *27*, 175–185.

Roos, J. *et al.* (2005). STIM1, an essential and conserved component of store-operated Ca^{2+} channel function. J. Cell Biol. *169*, 435–445.

Ross, K., Whitaker, M., and Reynolds, N. J. (2007). Agonist-induced calcium entry correlates with STIM1 translocation. J. Cell. Physiol. *211*, 569–576.

Samelson, L. E. (2002). Signal transduction mediated by the T cell antigen receptor: the role of adapter proteins. Annu. Rev. Immunol. *20*, 371–394.

Smyth, J. T., DeHaven, W. I., Bird, G. S., and Putney, J. W., Jr. (2007). Role of the microtubule cytoskeleton in the function of the store-operated Ca^{2+} channel activator STIM1. J. Cell Sci. *120*, 3762–3771.

Soboloff, J., Spassova, M. A., Tang, X. D., Hewavitharana, T., Xu, W., and Gill, D. L. (2006). Orai1 and STIM reconstitute store-operated calcium channel function. J. Biol. Chem. *281*, 20661–20665.

Spassova, M. A., Soboloff, J., He, L. P., Xu, W., Dziadek, M. A., and Gill, D. L. (2006). STIM1 has a plasma membrane role in the activation of store-operated Ca(2+) channels. Proc. Natl. Acad. Sci. USA *103*, 4040–4045.

Straight, A. F., Cheung, A., Limouze, J., Chen, I., Westwood, N. J., Sellers, J. R., and Mitchison, T. J. (2003). Dissecting temporal and spatial control of cytokinesis with a myosin II Inhibitor. Science *299*, 1743–1747.

Straus, D. B., and Weiss, A. (1992). Genetic evidence for the involvement of the lck tyrosine kinase in signal transduction through the T cell antigen receptor. Cell *70*, 585–593.

Szollosi, J., Damjanovich, S., and Matyus, L. (1998). Application of fluorescence resonance energy transfer in the clinical laboratory: routine and research. Cytometry *34*, 159–179.

Tskvitaria-Fuller, I., Rozelle, A. L., Yin, H. L., and Wulfing, C. (2003). Regulation of sustained actin dynamics by the TCR and costimulation as a mechanism of receptor localization. J. Immunol. *171*, 2287–2295.

Valitutti, S., Dessing, M., Aktories, K., Gallati, H., and Lanzavecchia, A. (1995). Sustained signaling leading to T cell activation results from prolonged T cell receptor occupancy. Role of T cell actin cytoskeleton. J. Exp. Med. *181*, 577–584.

Varnai, P., Toth, B., Toth, D. J., Hunyady, L., and Balla, T. (2007). Visualization and manipulation of plasma membrane-endoplasmic reticulum contact sites indicates the presence of additional molecular components within the STIM1-Orai1 complex. J. Biol. Chem. *282*, 29678–29690.

Vig, M. *et al.* (2006a). CRACM1 multimers form the ion-selective pore of the CRAC channel. Curr. Biol. *16*, 2073–2079.

Vig, M. *et al.* (2006b). CRACM1 is a plasma membrane protein essential for store-operated Ca^{2+} entry. Science *312*, 1220–1223.

Williams, R. T., Senior, P. V., Van Stekelenburg, L., Layton, J. E., Smith, P. J., and Dziadek, M. A. (2002). Stromal interaction molecule 1 (STIM1), a transmembrane protein with growth suppressor activity, contains an extracellular SAM domain modified by N-linked glycosylation. Biochim. Biophys. Acta *1596*, 131–137.

Wu, M. M., Buchanan, J., Luik, R. M., and Lewis, R. S. (2006). Ca^{2+} store depletion causes STIM1 to accumulate in ER regions closely associated with the plasma membrane. J. Cell Biol. *174*, 803–813.

Xu, P., Lu, J., Li, Z., Yu, X., Chen, L., and Xu, T. (2006). Aggregation of STIM1 underneath the plasma membrane induces clustering of Orai1. Biochem. Biophys. Res. Commun. *350*, 969–976.

Yeromin, A. V., Zhang, S. L., Jiang, W., Yu, Y., Safrina, O., and Cahalan, M. D. (2006). Molecular identification of the CRAC channel by altered ion selectivity in a mutant of Orai. Nature *443*, 226–229.

Yuan, J. P., Zeng, W., Huang, G. N., Worley, P. F., and Muallem, S. (2007). STIM1 heteromultimerizes TRPC channels to determine their function as store-operated channels. Nat. Cell Biol. *9*, 636–645.

Zalk, R., Lehnart, S. E., and Marks, A. R. (2007). Modulation of the ryanodine receptor and intracellular calcium. Annu. Rev. Biochem. *76*, 367–385.

Zhang, S. L., Yeromin, A. V., Zhang, X. H., Yu, Y., Safrina, O., Penna, A., Roos, J., Stauderman, K. A., and Cahalan, M. D. (2006). Genome-wide RNAi screen of Ca(2+) influx identifies genes that regulate Ca(2+) release-activated Ca(2+) channel activity. Proc. Natl. Acad. Sci. USA *103*, 9357–9362.

Zhang, S. L., Yu, Y., Roos, J., Kozak, J. A., Deerinck, T. J., Ellisman, M. H., Stauderman, K. A., and Cahalan, M. D. (2005). STIM1 is a Ca^{2+} sensor that activates CRAC channels and migrates from the Ca^{2+} store to the plasma membrane. Nature *437*, 902–905.